Chair of Reservoir Engineering

Master's Thesis

Sensitivity Analysis of the Trapping Potential of Different Rock Types using Digital Rock Physics

Lobel Zvonimir Danicic

March 2022

MONTANUNIVERSITÄT LEOBEN
www.unileoben.ac.at

AFFIDAVIT

I declare on oath that I wrote this thesis independently, did not use other than the specified sources and aids, and did not otherwise use any unauthorized aids.

I declare that I have read, understood, and complied with the guidelines of the senate of the Montanuniversität Leoben for "Good Scientific Practice".

Furthermore, I declare that the electronic and printed version of the submitted thesis are identical, both, formally and with regard to content.

Date 14.02.2022

Signature Author
Lobel Zvonimir Danicic

Lobel Zvonimir Daničić

Master 2022
Supervisor: Univ.-Prof. Dipl.-Phys. Dr.habil. Holger Ott
Co-supervisor: Dipl.-Ing. Pit Arnold

Sensitivity Analysis of the Trapping Potential of Different Rock Types using Digital Rock Physics

dpe DEPARTMENT PETROLEUM ENGINEERING

MONTAN UNIVERSITÄT

Dedicated to my loved ones

Declaration

I hereby declare that except where specific reference is made to the work of others, the contents of this dissertation are original and have not been published elsewhere. This dissertation is the outcome of my own work using only cited literature.

Name, 07 March 2022

Acknowledgements

I'd like to thank Prof. Holger Ott for the knowledge gained from him throughout my master's studies, as well as during the supervision of this thesis. Simple, yet effective explanations of the complex topics are something I'll remember. Next, I'd like to thank Pit Arnold, who has also helped me throughout the courses and in development of my master thesis. Many insights about proper methodology and explanations are something I'll take with me.

I'd like to thank the rest of the Chair of reservoir engineering and colleagues for the knowledge transferred and help provided. These particularly include Ms Bettina Matzer, Patrick Jasek, and Mario Stefan Dragovits.

Many thanks to the rest of my friends who supported me in all possible ways.

Finally, I want to thank my dear family for all the help, love and understanding throughout my complete education. Without you, it would be impossible. Last, I am grateful to my dear Valentina for all the support, love and strength that has guided me to persist and continue.

Abstract

Carbon Capture and Storage (CCS) is one of the few options to store carbon dioxide on a large scale and therefore actively reducing greenhouse gas emissions. Thorough knowledge of reservoir properties and trapping mechanisms is needed to ensure the most proper application while ensuring maximum storage safety. Fluid-fluid and rock-fluid properties are assessed from routine and special core analysis programs (SCAL), from which displacement and trapping efficiencies can be derived. However, SCAL experiments take a considerable amount of time and effort. Advances in computational power and imaging techniques in the field of Digital Rock Physics (DRP) enable the simulation of capillary trapping processes within a reasonable time frame, while varying reservoir properties. Using experimental data as calibration it allows the computation of different fluid-fluid and rock-fluid combinations. This thesis focuses on the simulation of capillary trapping curves for the evaluation of the carbon dioxide trapping potential for different rock types.

The used simulation tool is GeoDict in particular its module Satudict, which models drainage and imbibition processes based on the morphological method. The investigation includes six different digital twins of real sandstone rocks to observe the effect that the different pore structures have on the capillary trapping. To compute the trapping potential of a rock type a drainage process is performed, followed by imbibition scanning curves. Subsequently the residual non-wetting phase (NWP) saturation is evaluated. As the imbibition process is of major interest, two approaches are used for its modelling. Whereas the first approach is limited to spontaneous imbibition only, while the second one incorporates the full imbibition branch including the forced imbibition. Obtained capillary pressure results with both imbibition modelling approaches are then analysed with the Land model. The investigation includes the analysis of alternating wetting conditions.

The results show that the rock type and wettability have the largest influence on the trapping potential. Furthermore, it was shown that domain size and capillary end effects majorly influence the results, indicating that larger domains are favourable. In addition, the correlation between the rocks petrophysical properties and their trapping potential was investigated. It was shown that the pore size distribution in combination with the pore throat size distribution correlates with the trapping potential.

Zusammenfassung

Carbon Capture and Storage (CCS) ist eine der wenigen Möglichkeiten, Kohlendioxid in großem Umfang zu speichern und damit Treibhausgasemissionen aktiv zu reduzieren. Umfangreiche Kenntnisse der Lagerstätteneigenschaften und Speichermechanismen ist erforderlich, um die ordnungsgemäße Anwendung bei gleichzeitig maximaler Lagersicherheit zu gewährleisten. Die Eigenschaften zwischen den Flüssigkeiten und dem umliegenden Gestein werden anhand von routinemäßigen und speziellen Kernanalyseprogrammen (SCAL) untersucht, von diesen können dann Fließ- und Speichereffizienzen abgeleitet werden. Allerdings nehmen SCAL-Experimente viel Zeit und Mühe in Anspruch. Fortschritte in der Rechenleistung und bildgebenden Verfahren im Bereich der Digitalen Gesteinsphysik (DRP) ermöglichen die Simulation von Kapillarphysikprozessen innerhalb eines angemessenen Zeitrahmens bei gleichzeitiger Variation der Lagerstätteneigenschaften. Mit Hilfe experimenteller Daten werden die Modelle kalibriert, was die Simulation verschiedener Gesteins- und Flüssigkeitskombinationen ermöglicht. Diese Arbeit konzentriert sich auf die Simulation von kapillaren Druckkurven zur Bewertung des Kohlendioxidspeicherpotentials für verschiedene Gesteinsarten.

Die verwendete Simulationssoftware heißt GeoDict, wobei insbesondere dessen Modul Satudict, welche Drainage und Imbibition Prozesse auf der Grundlage der morphologischen Methode modelliert. Die Untersuchung umfasst sechs verschiedene digitale Gesteinszwillinge, um zu untersuchen wie sich die unterschiedlichen Porenstrukturen auf die Kapillardruckkurven auswirken. Um das Speicherpotential einer Gesteinsart zu berechnen, wird ein Drainage Prozess durchgeführt, gefolgt von Imbibition-Scanning-Kurven. Anschließend wird die Restsättigung der nicht benetzenden Phase (NWP) ausgewertet. Da der Imbibitionsprozess von großem Interesse ist, werden zwei Ansätze für dessen Modellierung verwendet. Während der erste Ansatz nur auf spontane Prozesse beschränkt ist, umfasst der zweite den vollständigen Imbibition Zweig einschließlich der forcierten Verdrängung. Die erhaltenen Kapillardruckergebnisse aus beiden Modellierungen werden dann mit dem „Land model" analysiert. Die Untersuchung umfasst dabei auch die Analyse unterschiedlicher Benetzungszustände.

Die Ergebnisse zeigen, dass die Gesteinsart und Benetzungseigenschaften den größten Einfluss auf das Speicherpotential haben. Darüber hinaus wurde gezeigt, dass die Domänengröße und Kapillare Endeffekte die Ergebnisse stark beeinflussen, was darauf hindeutet, dass größere Domänen vorteilhafter sind. Darüber hinaus wurde die Korrelation zwischen den Petrophysikalischen Eigenschaften der Gesteine und ihrem Speicherpotenzial untersucht. Es

zeigte sich dabei, dass die Porengrößenverteilung in Kombination mit der Porenhalsgrößenverteilung am meisten korreliert.

Table of Contents

List of Figures

xii

List of Tables

Nomenclature

m	mass	[kg]
r	radius	[m]
σ	interfacial tension	[N/m]
θ	contact angle	[°]
C	Land-model parameter	[-]
P_c	capillary pressure	[Pa]

Abbreviations

CCS	Carbon Capture and Storage
PMM	Pore Morphology Method
IFT	Interfacial Tension
DRP	Digital Rock Physics
REV	Representative Elementary Volume
CA	Contact Angle
WP	Wetting Phase
NWP	Nonwetting Phase
WW	Water-wet
OW	Oil-wet
NW	Non-wet
IR Curve	Initial-Residual Curve
SVP	Solid Volume Percentage
PSC	Pore Space Considered
TORS	Turn Oil Rock Surface

Chapter 1

Introduction

In the current context of climate changes and how the petroleum industry can mitigate the effects of fossil fuels, Carbon Capture and Storage (CCS) seems to be one of the most promising solutions. Possible applicability is in depleted oil reservoirs and the deep saline aquifers. Over considerable time periods, capillary trapping plays substantial role in the overall process. The carbon dioxide (CO_2) storage safety and potential is dependent on the geological trapping structures and the reservoir rock type. Capillary trapping, as one of the major mechanisms, is evaluated by the residual CO_2 saturations that largely depend on the rock's pore structure and wettability. Trapped saturations depend on initial CO_2 saturations reached during the drainage. SCAL experiments are conducted to evaluate the potential CCS reservoirs. In such studies, multiple experiments have to be conducted to describe the hysteretic saturation cycles, which is time-consuming and can oftentimes be complex. Another issue is that a rock sample used in the experiments can oftentimes exhibit heterogeneous behaviour not valid for the whole reservoir system. This would make the obtained experimental results not valid for CCS assessment. Therefore, it would be useful to have many rock samples for the adequate reservoir description. That, on the other hand, is impossible due to tremendous efforts, high costs, and various complexities of the coring and laboratory analysis. With the advance of Digital Rock Physics (DRP) and reduction of computing times, the difficulties related to experimental SCAL methods are tackled. Although still far from perfect, the digital rock computing enables the investigation of different processes in porous media in the swift and repetitive manner. A such investigation in this thesis is focused on the impact of different rock types on the capillary trapping.

1.1 Background and Context

Theoretically, uncertainty modelling that is part of DRP allows a better description of the reservoir heterogeneities' impact, and thus yields a more representative conclusion for potential CCS screening application. However, the question is whether it is possible to use such a digital environment appropriately, as there are certain limitations to the currently-used calculation methods used in DRP.

Adequate description of capillary trapping requires valid drainage and imbibition modelling. Imbibition is of particular importance, as invasion of wetting phase (WP) makes the non-wetting phase (NWP) trapped. This particularly happens during hysteretic saturation cycles. Pore morphology method, which is implemented in module Satudict of software Geodict used in this thesis, uses morphological approach to describe drainage and imbibition processes. Initially, it could only model spontaneous imbibition. This may have led to inadequate description of capillary processes, thus resulting in unexpected behaviour and residual non-wetting saturations. This limitation has recently been tested with a newly-developed Forced Imbibition macro, promising the more accurate description of the hysteretic capillary pressure cycles by implementing the full imbibition branch (spontaneous and forced). To assess the further potential, both the modelling of spontaneous and forced imbibition is part of this study so that a clear distinction is obtained on the impact of imbibition modelling approach. Subsequently, assessment of trapping potential is done with application of foundational Land model. Generally, Land model is matched to hysteretic initial-residual (IR) saturation pairs reached during drainage and imbibition experiments. Here it is applied to the simulated IR pairs.

The results of described workflow are presented in this thesis. Influence of the rock structure is investigated, as well as the imbibition modelling approaches. The simulated results are assessed whether they have physical meaning, and this is done by comparing with literature data that consists of wide range of different sandstone trapping curves. Additional investigation of domain size modification gives the possibility to tackle the shift from pore to macro-scale. Furthermore, a major implication is in impact that pore structures have on trapping potential. Therefore, relationship with structures' petrophysical properties is addressed as a part of quantitative results' validation.

1.2   Scope and Objectives

This thesis is focused on investigation of DRP capabilities for assessing the capillary trapping potential of different rock types. Two approaches for imbibition modelling, namely spontaneous and forced imbibition, are used. Different sandstone digital rock structures are utilized. In the investigation scope is the alteration of rocks' initial wetting conditions with the variation of contact angle and secondary material of NW properties. This approach adds the uncertainty modelling of wetting properties onto the rock structures and pore geometries utilized. Obtained capillary pressure curves are further described with Land trapping model, and results are compared to literature data as a qualitative benchmark. Issue of domain size is tackled with additional investigation and domain modification. Final consideration correlates the impact of pore geometry with the observed trapping potential.

Chapter 2

Literature Review

Before delving deeper into the technical part with the simulation workflow and the results' presentation, it is important to obtain the better understanding of underlying processes, analysing tools, and computational approaches. First, the process of CCS through the lens of pore physics involved is summarized from the literature, as that is the key motivation in this work. Next, Land Trapping model is discussed and explained, as it is the empirical tool to benchmark results in this study. Next, the background of Digital Rock Physics in the context of pore morphology method is elaborated as this study's key solving approach of the proposed issues. The experimental results from literature are screened and discussed as the quality check that will be used in setting the parameters for the simulations in this study.

2.1   Carbon Capture and Storage

The burning issue of CO_2 emissions feels every day more present. The need to cut the emissions, and what to do with the produced CO_2 are just some of the most frequent questions in the scientific areas related to this topic. The Carbon Capture and Storage/Sequestration is one of the possibilities of the emissions' reduction, where the petroleum industry can drastically make an impact. The reason of elaborating in detail on CCS and physics behind is to establish the pros and cons of this thesis' workflow and the tools used. By acknowledging the experimental and theoretical conclusions so far from different authors, the assessment of various implications will be done and what are the potential limitations of this work.

Reasons why CO_2-related issues can be tackled by oil industry are the long history of established theoretical principles and empirical knowledge gained in dealing with CO_2. Followingly, when it comes to CCS, it is the oil industry that knows the best all the similarities and differences between the crude oil and CO_2. Therefore, some of the CO2 properties that are of interest for this thesis will be compared to those of oil. As the literature review has shown, IFT of brine-CO_2 system is comparable to that of brine-oil system, having values from 30 to 45 mN/m on average (Saraji et al. 2013). Next, contact angles observed in CO2-brine systems are, as well as IFT, considerably comparable to the ones observed in oil-brine systems. The literature screening has shown that similarly to oil, there's the wide influence of both the rock type and the reservoir

conditions on the contact angle observed. Conclusively, general trend can be drawn between the two systems and therefore it is an additional affirmation of oil industry's importance in CCS Research & Development.

Next, historical examples of CO_2 studies and application in the oil industry can show the future potentials. The research of CO_2-EOR started back in 1950s, when Whorton, Brownscombe, and Dyes were granted patent for the technology (Whorton et al. 2021.). Soon following, other scientists continued the research, and first field-scale projects were conducted, starting in 1964 at Mead Strawn Field (Holm et al. 1971). By injecting CO_2 into the oil reservoir, it was discussed that substantial amount of CO_2 could be stored in the oil reservoirs. Development of CO_2 for EOR continued; however, with the environmental issues arising in the context of climate changes, its sequestration in the reservoirs gained additional attention. To sequester larger quantities, next step was to investigate further the storage of CO_2 in the saline aquifers, as they seemed to be the largest reservoirs available. However, due to much larger historical exploration for oil reservoirs and their overall characterization, as well as the developed infrastructure, it is mainly to be expected that most of the forthcoming CCS projects will be developed in the previously developed oil reservoirs. The first large-scale CCS project, where decrease of CO_2 atmospheric emissions is the key driver due to governmental tax, is the Sleipner Project in Norway. CO_2 is removed from natural gas and re-injected into the saline aquifer (IEA 2021.). The overview of existing and planned CCUS facilities in 2021 was done by International Association of Oil and Gas Producers (IOGP) and Global CCUS Institute (IOGP Publications library 2021.). Resulting map with count of projects per continent can be seen in Figure 1.
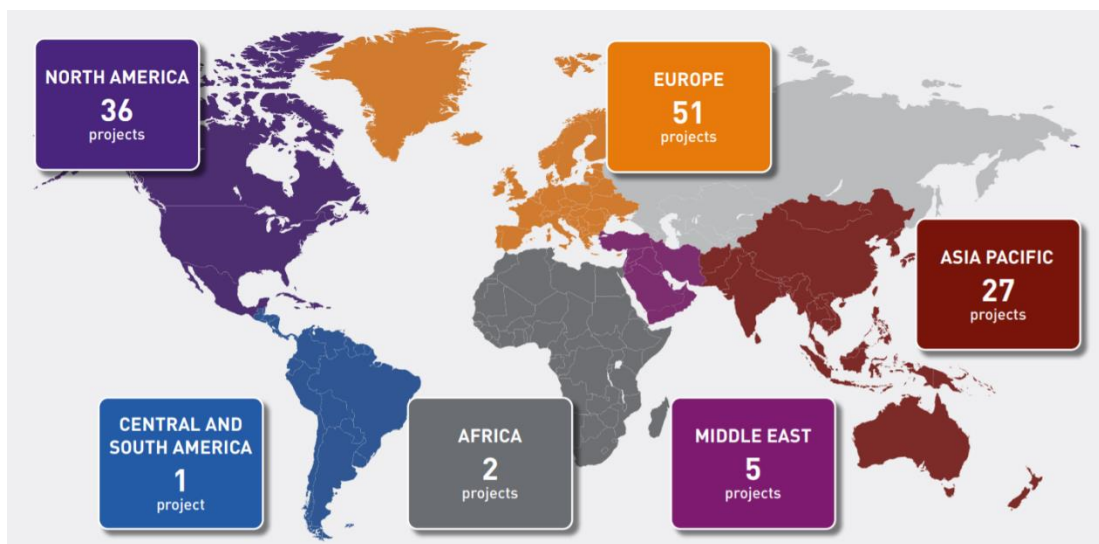
Figure 1. Overview of global existing and planned CCUS facilities as of April 2021 (IOGP Publications library 2021.)

To assure the safer long-term storage of CO_2, the deeper investigation has to be done of various interactions between brine, rock, oil, and CO_2. This led to questions such as: what are the mechanisms of carbon dioxide trapping in the reservoir, and how much of it can be effectively stored? They include structural and/or stratigraphic trapping; residual/capillary trapping; solubility trapping, and mineral trapping. All the mentioned mechanisms should combinedly secure the trapping of injected carbon dioxide; for example, if there is no geological structure to assure safe storage in the potential reservoir, field-scale projects most likely won't be considered due to possible leakages to shallower layers.

2.2   Capillary Trapping

The focus of this work is on the mechanism of capillary trapping. Capillary trapping can be described as the residual saturation of the non-wetting phase in the porous medium after the imbibition of the wetting phase. Key factors influencing it are wetting properties of the porous medium, interfacial tension between two non-miscible fluids, and the size of pores, namely pore throats, as described with following Young-Laplace (YP) equation:

$$P_c = \frac{2\sigma cos\theta}{r}$$

, where P_c is capillary pressure in Pa, σ is the IFT between brine and CO_2 in N/m, θ is the contact angle (degrees), and r is the pore throat radius (micron). According to Young-Laplace equation, larger interfacial tension increases the capillary pressure between the wetting and non-wetting phases. Smaller pore throats have increasing effect on capillary pressure too. Further, one of the crucial mechanisms in description of capillary trapping at pore-scale includes wetting phase (WP) snap-off. This is a process of swelling WP film during the imbibition, that results in sudden increase of capillary pressure at pore throats according to YP equation. Subsequently, NWP gets trapped in the pore centres. It is visually given in Figure 2:
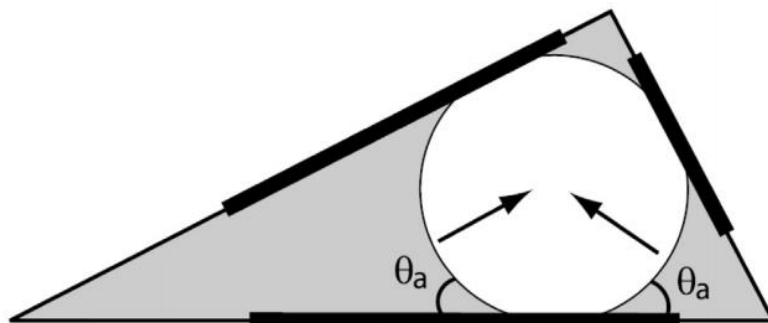
Figure 2. Pore-filling and subsequent snap-off of the wetting (grey) layer around non-wetting droplet (white). Notice that the limiting, trapping factor of the non-wetting droplet is the pore throat size, which limits its transport to the next pore due to capillary forces being stronger than buoyant. Figure taken from (Valvatne and Blunt 2004) .

The importance of capillary trapping as the storage mechanism is in transition from purely physical, shorter-term trapping, towards the long-term geochemical assurance of trapping safety, especially in the saline aquifers where sometimes no adequate physical structure is to be found. This transition of trapping mechanisms has been discussed in a number of works, such as (W. Gunter et al. 1993; Benson and Orr 2008), and can be seen in the Figure 3.
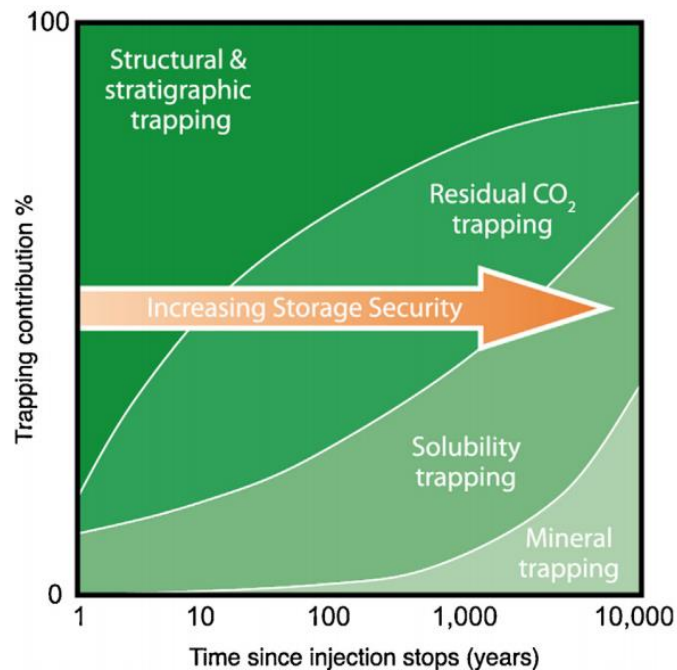
Figure 3. Trapping mechanisms of CO2. The change from the physical to geochemical trapping is seen as the time advances. After Benson et al. (2005, 2012).

As Krevor and his team elaborated, capillary trapping has been recognized as crucial both due to its total extent and the time scale at which it leads to the efficient trapping (Krevor et al. 2015). With the topic gaining in popularity, the advance of research was observed in the last two decades, where numerous authors have come up with several conclusions in experimental and numerical investigations. Their work included understanding the most basic – smallest – scale and how the numerous effects interplay as the scale increases from pore to core, and eventually the field level (Krevor et al. 2015).

To understand the fluid displacement mechanisms at the pore scale, one of the tools pioneered that scientists use is micromodel flooding (Lenormand et al. 1983). This enabled the observation of the flow-related phenomena, such as the pore-to-pore displacement and preferential filling of larger pores first by the nonwetting phase (CO_2). Next breakthrough in the field of pore-scale flow description was the use of synchrotron X-ray devices, namely µCT and medical CT scanners. These tools enabled the tracking of flow profile propagation along the rock sample, leading to additional description previously attainable only in the transparent models (Krevor et al. 2015; Blunt et al. 2013). Having said that, it is important to describe the key processes

describing the capillary trapping more in detail. These are wetting layer snap-off and piston-like advance of the fronts. Piston-like front can be described as the preferential filling event of pore throats if there is only one throat to be filled compared to two or three throats. This is coming out of the Young-Laplace equation, and the impact comes from the radius of curvature – if more of the pore throats have to be filled, radius of curvature will be higher, meaning that water imbibing pressure has to be higher too (Krevor et al. 2015). This can be seen in Figure 4.
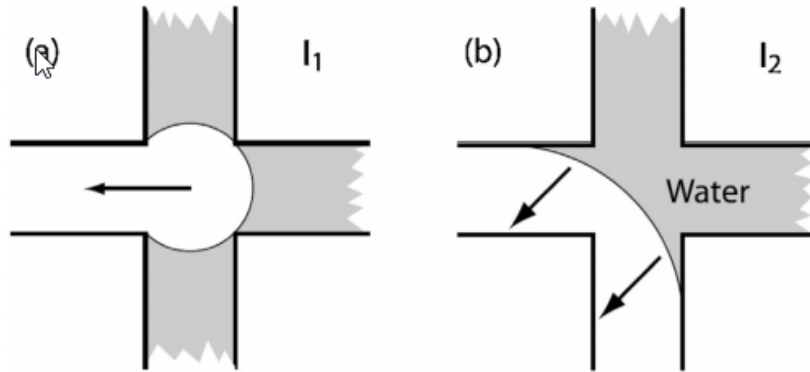
Figure 4. Wetting phase (grey) imbibing and pushing the non-wetting phase from a) a pore connected only to one throat, b) from a pore connected to two throats. The latter case is occurring at lower capillary pressure, which is less favoured displacement-wise for the wetting phase (water). Therefore, a) case is more possible and will result in the piston-like displacement (Krevor et al. 2015).

Now, the real question arose in the context of applying the mentioned effects on the actual trapping mechanism of CO_2. The main concern is the wettability influence on the trapping safety and capacity. If the rock is mixed or even CO_2-wet, the mentioned processes of wetting layer snap-off and/or piston-like advance will possibly not occur (Krevor et al. 2015). Therefore, many authors focused on exploring the wetting properties of the rock.

Regarding the wettability, various parameters such as CO_2-brine surface tension have been tackled in (Xing et al. 2013); capillary-viscous-gravity force balance in varying reservoir conditions; the effectiveness of trapping in the mixed-wet oil reservoirs vs. water-wet (Al-Menhali and Krevor 2016), etc. Interestingly, there are differing conclusions about the dependencies of contact angle as the wettability parameter vs. pressure, salinity, and/or temperature. The reasons include complex and variable experimental conditions between different laboratories, resulting in the non-recognizable various "side effects", such as CO_2-surface roughness interplays, the obtainable resolution, etc. Even though the end results and conclusions about the trapping efficiency can therefore vary by an appreciable amount, the key takeaways do not significantly change. Over the wide range of experimental data provided in the works of (Bennion and Bachu 2008; Pentland et al. 2011; Hu et al. 2017; Ruprecht et al. 2014; Krevor et al. 2012; Akbarabadi and Piri 2013; El-Maghraby and Blunt 2013; Niu et al.

2015), significant agreements exist between authors' Initial-Residual (IR) rock-characteristic curves. This assumes that the robustness of the curve type is consistent over the range of conditions, and maybe even across varying experimental procedures (Krevor et al. 2015).

2.3 Initial-Residual saturation relations and Land model

Next, it has to be explained what the Initial-residual (IR) curve actually is. It comes out after the pore-scale description of CO_2 trapping. After pore-to-pore approach, next step is "upscaling" the magnitude - averaging the pore-to-pore effects to the centimetre scale of core sample. This has historically been done to describe the core/reservoir trapping properties when producing the gas (Land 1968), whereas its purpose now is in other direction – describing the core's CO_2-trapping capabilities for CCS. This endeavour resulted in the realization of empirical relations between the amounts of initial and residual nonwetting phase saturations (Krevor et al. 2015). One such work, taken as the staple for further empirical developments, was proposed by Carlon S. Land.

By combining the previous knowledge of relative permeability dependence on the pore size and the saturation pathway of non-wetting phase, Land developed empirical model that relates initial NWP saturation to residual NWP saturation, specific to a certain rock sample. He plotted the data from several experimental studies and the curves for each rock sample seemed to exhibit a characteristic shape, which can be seen in Figure 5 (Land 1968). Then he fitted the model, noting the clear trend between initial and trapped non-wetting saturation. Experiments are done for several initial/residual turning saturation pairs. At a certain saturation achieved during drainage, imbibition flood is started. This is done at several saturation points, and every time, imbibition flood is done until the residual NWP saturation. This approach results in the hysteretic model and so-called scanning curves, which was first mentioned by (Killough 1976). Hysteretic behaviour will be one of the focuses in this thesis, as capillary trapping relies on it. There is the lower ratio of residual NWP saturation as the initial NWP saturation increase. This depicts how lesser amounts get trapped effectively, namely due to the higher intrusion into the progressively smaller pores (Krevor et al. 2015). Also, one conclusion would be that these smaller pores would be first in line for WP re-saturation, particularly in the water-wet rock, once the imbibition takes place. The characteristic behaviour of each rock sample is captured in the coefficient C. The behaviour between the trapped saturation and coefficient C is reciprocal as can be seen in Equation 1:

$$S_{CO_2}^*, r = \frac{S_{CO2}^*, i}{1 + C S_{CO2}^*, i}$$

Equation 1. IR model proposed by (Land 1968). CO_2 initial and residual saturations are normalized to the irreducible water saturation, and C coefficient is sample-specific.
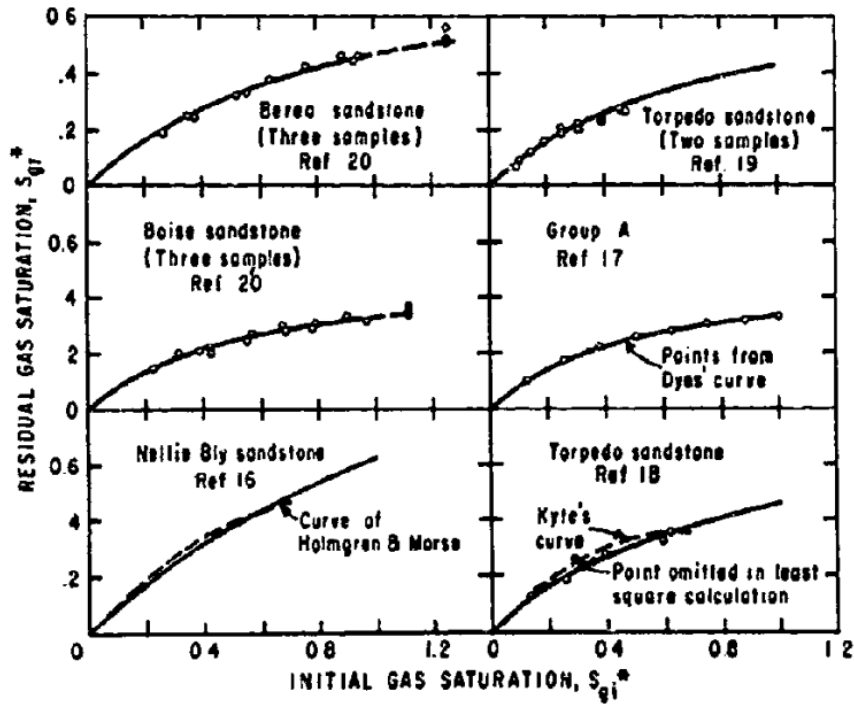
Figure 5. Original trapping curve fits done by Land to published experimental data from different authors (Land 1968). Note that plot axis limits are not same for each example. Also, axes show normalized initial and residual saturations which can be greater than 1 for samples initially not containing any water.

One of the remarks from Spiteri and her team is that Land model, even though is the key concept and most used, describes unrealistically the intermediate and/or oil-wet rocks (Spiteri et al. 2008). It doesn't capture the realistic nonmonotonic behaviour of trapping curves with the increase of NWP saturation, nor does it accommodate for the relative permeability scanning curve crossing in intermediate/oil-wet media. Anyhow, Land model is satisfyingly precise in water-wet media and simple to apply in conjunction with other models, such as with hysteretic models from various authors, such as (Killough 1976; Lenhard and Oostrom 1998; Larsen and Skauge 1998; Blunt 2000). Therefore, Land model will be used in this study as well, as it is effective and makes a strong qualitative benchmark of trapping capabilities.

Considering different rock samples in the multitude of experiments from various authors, Krevor and his team established the database with bottom and top limits of Land-parameter C based on the level of heterogeneity (Krevor et al. 2015). When only experimental results with Berea sandstone are plotted, range of C is significantly lower – from 0.7 to 2 – whereas the range including the results from carbonate experiments varies from 0.2 to 5 (Krevor et al. 2015), as seen in Figure 6. This extensive difference between these rocks arises from well-known carbonate heterogeneity, such as change in wettability – from mixed-wet to highly water and/or oil-wet regions – due to divalent cations in its minerals; zones containing significant fractures

vs. extremely low-permeability matrix, etc. Therefore, conclusion can be derived that in carbonate reservoirs, there could be significant differences of capillary CO_2 trapping between different parts of same reservoir. The deeper dive into the database will be done in one of the next chapters.
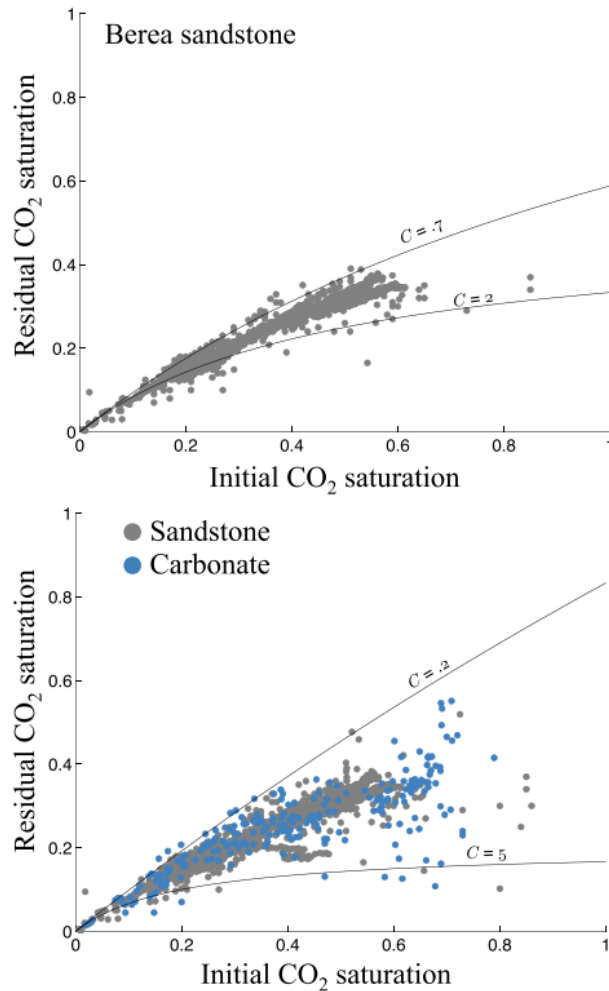
Figure 6. Upper plot shows the IR trapping results from literature brine-scCO2 experiments in sandstone. Lower plot includes both sandstone and carbonate experiments. Solid lines show the fit of Land model trapping curves that include approximately 95% of data. From (Krevor et al. 2015).

Mainly experimental and numerical data gathered so far from various studies will be used to sensitivity-test the results obtained in software from Math2Market, Geodict 2021. Geodict was used to simulate primary drainage-imbibition experiments on different digital rock samples. Simple Geo-Python scripts were written to automate the simulation process and also to simulate imbibition-drainage scanning curves. Rock-fluid properties were varied in effort to recreate diverse, stochastic results while maintaining the properties published experimental data. Geodict relies on pore morphology method, which operates on YP capillary-pressure equation

algorithm for the determination of saturation distribution in the porous medium. As such, there are certain opportunities and limitations that will be discussed next.

2.4 Pore morphology method for capillary pressure modelling

Pore morphology method, or full morphological method, is the approach developed on the concepts of mathematical morphology and applied on the porous media, as first mentioned in works of (Bakke and Øren 1997; Bryant et al. 1993; Hazlett 1995; Hilpert and Miller 2001). Its premise relies on morphological operators of dilation, erosion, and opening. Further, often-used naming convention is the Minkowski addition and subtraction for dilation and erosion, respectively. These operators are based on geometrical processes including two or more objects. For simplest illustration of mentioned operators, following Figure 7 is presented. Combining the morphological approach with the sphere-type object, application was found in capillary pressure calculation. As YP equation for capillary pressure shows, the increment or decrement of radius of curvature changes the pressure. Applying this approach on the 3D images of porous media with a spherical object, one can deduct the pore size and capillary thresholds of a certain porous medium. But first, the following steps will explain the workflow of the first iteration of algorithm used in Geodict, developed by Hilpert and Miller (Hilpert and Miller 2001).

Initially, the digital porous medium is inhabited by the wetting phase. NWP reservoir(s) is located on one of the model's borders. From it, NWP phase in the spherical form will start intruding the digital porous medium by eroding the WP from rock grains. As the capillary pressure increases via decrease of radius of spheres, the smaller pores are invaded. As the pores are filled from NWP reservoir, it is important that the NWP phase stays connected to the reservoir to establish the certain capillary pressure related to the current step of intruding sphere diameter. The complete algorithm relies on three mentioned morphological operators; erosion, dilation and opening. The process can be seen in Figure 8 (Hilpert and Miller 2001).
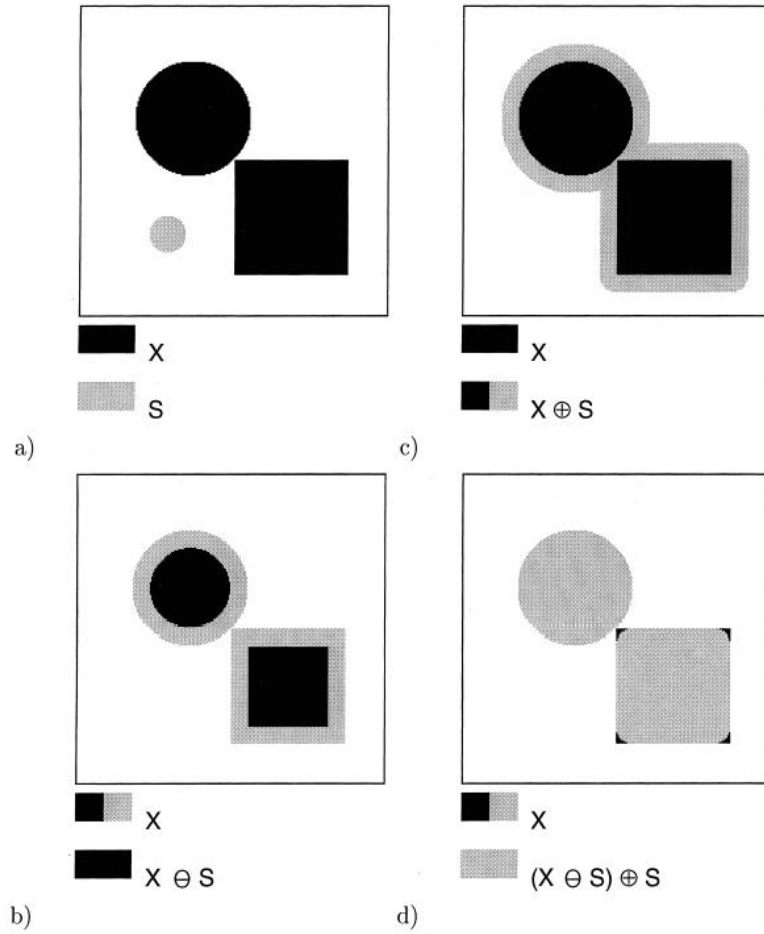
Figure 7. Morphological operations in two dimensions: (a) set X and sphere S; (b) erosion E of X by S; (c) dilation D of X by S; (d) opening O of X by S. From (Hilpert and Miller 2001).
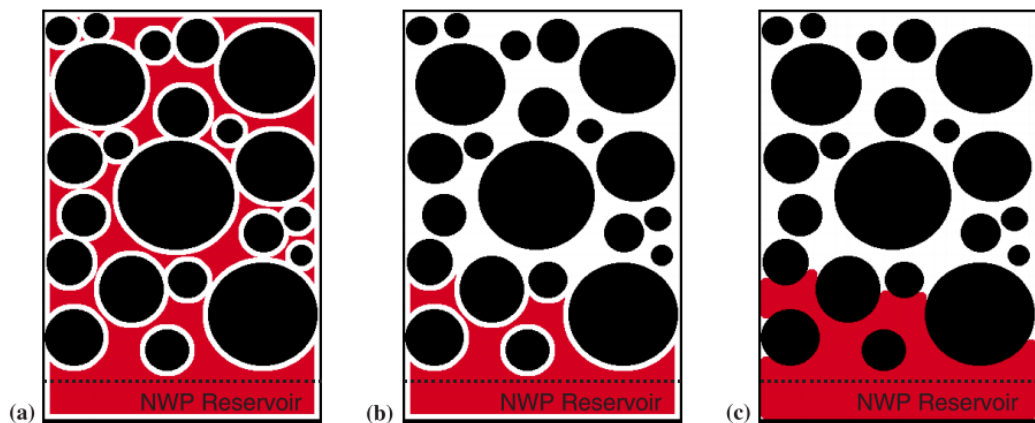
Figure 8. Representation of original 2D illustration of drainage simulation. Note the invasion from bottom. Black spheres represent the solid material. In a) the pore space, in red, is eroded by sphere (circle in 2D), and b) only the NWP phase in pore space connected completely to the NWP reservoir remains for this step, where in c) the solid/NWP interface is reshaped according to the proposed contact angle (Hilpert and Miller 2001).

However, this approach is not considered as the ideal representation of capillary pressure. As was investigated by Berg and his team, the morphological approach used in Geodict does not incorporate the ganglion dynamics flow mechanisms, such as wetting-layer snap-off, piston-like displacement of NWP, their competition and subsequent entrapment of NWP (Berg et al. 2016). These mechanisms are observed on the continuum-scale of rock, and as such are not recognized in morphological method, which considers only the local, pore-to-pore scale. Anyhow, the results from drainage simulations are considerably correct, whereas imbibition-simulation results are as well satisfying at lower wetting-phase saturations, as the comparison has shown between experiments and simulation (Berg et al. 2016). Also, it is important to mention that current approach in calculating imbibition is based on reverse drainage – swapping the contact angles between two phases and proceeding until the residual saturation.

From the presented literature findings of pore-scale physics in CCS and the explanation of morphological method, the following can be established regarding the application of morphological approach for the purpose of CO_2 trapping investigation.

First, the effect of CO_2-brine experimental conditions is inconsistent once the supercritical state is achieved, and there are different observations of influence of properties such as temperature, pressure, and salinity. Morphological approach doesn't directly incorporate nor rely on any of these effects, rather only the wetting state of the porous medium is concerned. Next, capillary trapping was shown as mainly governed by the pore structure and wettability of the media, and these properties are directly incorporated in the morphological approach. Also, there is no direct incorporation of imbibition trapping mechanisms of piston-like displacement and snap-off in the morphological approach. These processes are considered at the macro-scale of structure, and morphological approach doesn't resolve them at the pore-scale. Anyhow, these flow mechanisms have been experimentally demonstrated as minor if the reservoir wetting state is moved towards neutral or CO_2-wet. Anyhow, the mentioned limitations have to be acknowledged.

Next, the scale of the simulation results has to be considered. As these simulations are run at the micro scale (10^{-6} m), their comparison to experimental results at macro, centimetre scale may be invalid. Proper upscaling issue from micro to macro should be tackled, and clearly expressed.

2.5   Experimental data from literature

Geodict allows the user to adjust certain parameters – contact angle(s), IFT – for capillary pressure simulations. To use the proper values, the real-life experimental results were used from different authors and here presented. Although the mentioned parameters in realistic environment depend on other factors – such as salinity, pressure, temperature – whose impact is here only presented (Figure 9), while it bears no influence in Geodict as there is no incorporation of thermodynamic processes. However, the influence is not dramatically impactful, therefore for the simulation purposes it can be effectively ignored. Finally, a screening of database Land-model coefficients is presented too, as it will serve for comparison with the simulated results in this thesis.

Contact angle

Farokhpoor and team conducted experiments trying to measure contact angles of different minerals (quartz, calcite, muscovite) and varying brine salinity, initial pressure and temperature (Farokhpoor et al. 2013). Their results have shown variation in contact angle regarding every of the mentioned parameters and can be seen in Figure 9. The general trend for every mineral type can be concluded, and it is that pressure influences the contact angles up to the critical point, and later its influence is only minor (can be considered as none). Also, with higher salinity, minerals have shown slightly lower wettability. Next, the temperature influence varies depending on the mineral observed, being none or considerable.
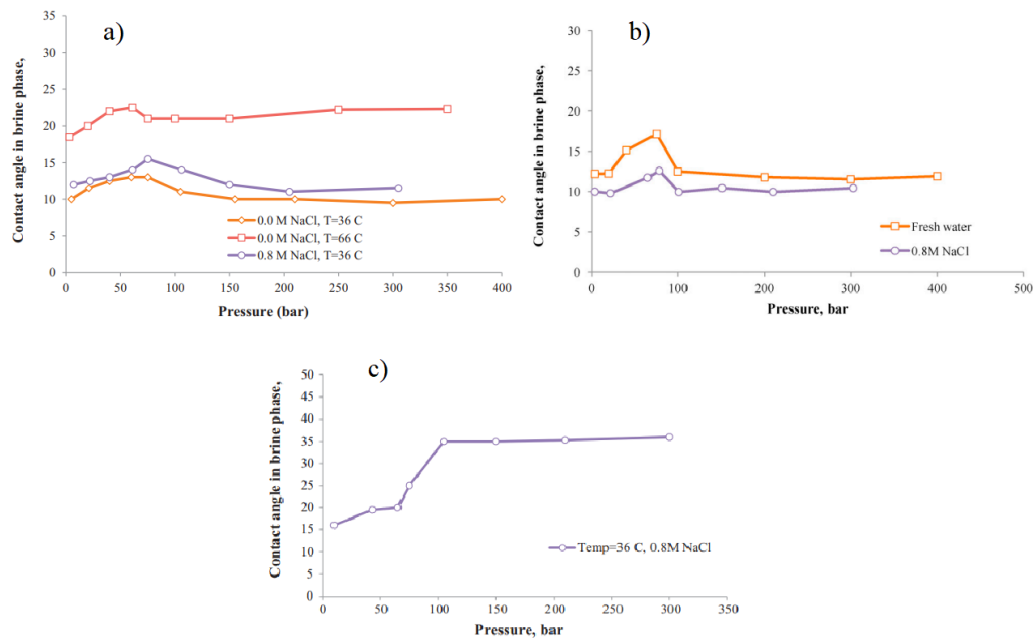
Figure 9. a) CO2-brine contact angle on calcite, b) CO2-brine contact angle on quartz surface, c) CO2-brine contact angle on muscovite mica. All three plots relate contact angle on y-axis to pressure on x-axis. From (Farokhpoor et al. 2013).

Further, the work of Saraji and team shows the similarity with the results obtained from Farokhpoor and team study for quartz (Farokhpoor et al. 2013). As can be seen in Figure 10, contact angles obtained in both works are comparable and range from 10°-40°. To add a different approach based on fitting the data, the work of (Al-Menhali and Krevor 2014) was investigated. Their results come from fitting MICP curve to CO2-brine system by applying the IFT of 34.5 mN/m and sensitivity range contact angle/s of 50°+-10°. By comparing their experimental results of saturation-to-pressure to the fitted MICP curve, they have come up with a strong fit, meaning that the values they came up with in fitting process can be taken as appropriate. Therefore, the values to be used in the simulations can be derived from this and previously mentioned works, taken as the commonly observed values. Also, similar values were observed in works of other authors.
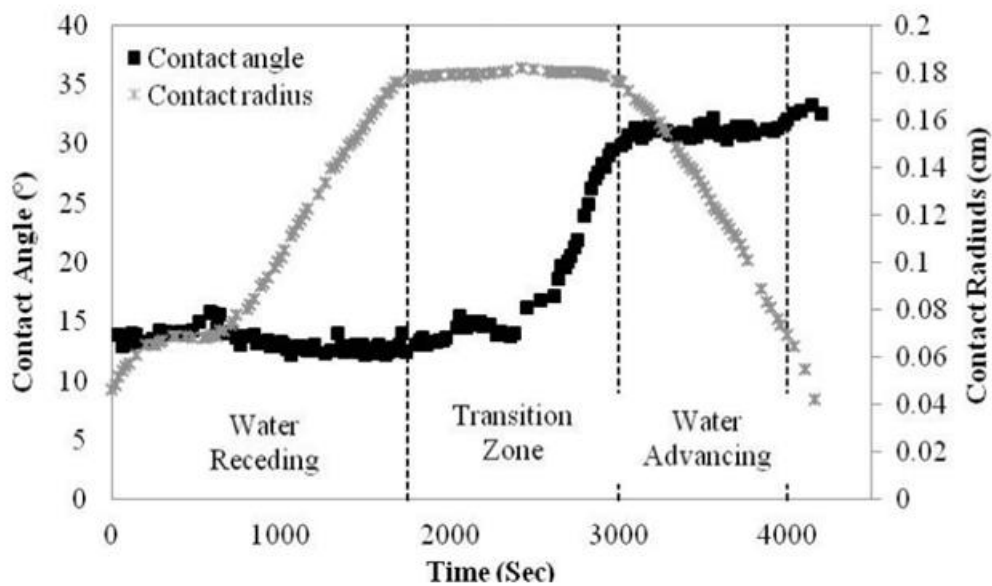
Figure 10. Receding and advancing contact angle results for CO2 bubble on quartz in water at 1700 psi and 60°C. From (Saraji et al. 2013).
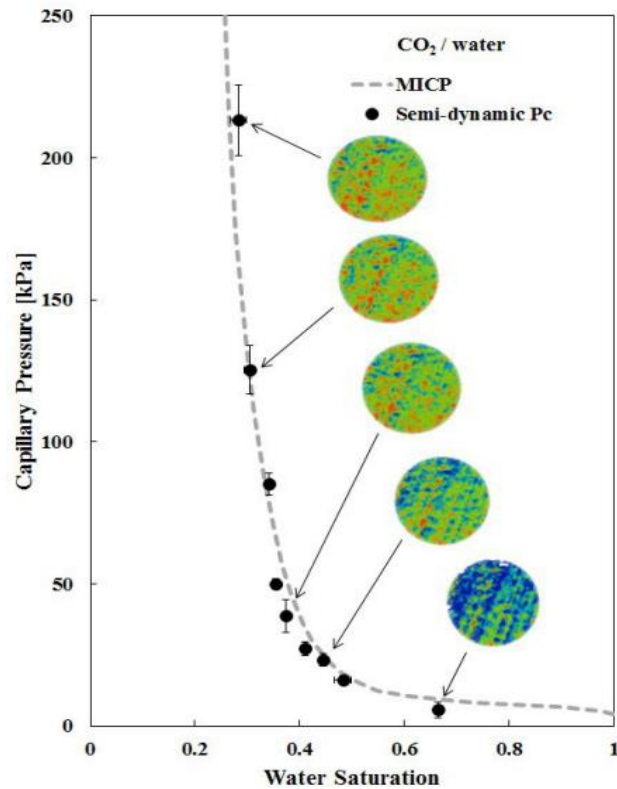
Figure 11. An example of a CO_2-water capillary pressure experiment (black dots) from (Al-Menhali and Krevor 2014). Black dots represent the experiment (14 MPa, 60°C and 1 mol/kg brine), while the dotted line is the best fit of MICP experiment scaled with IFT of 34.5 mN/m and contact angle of 50°. Also, CT scans are presented showing the CO_2-brine at selected saturation steps.

Interfacial Tension

For EOR, the influence of interfacial tension is significant and oftentimes one of the key parameters to investigate (Pit Arnold 2018). However, the IFT serves only as the scaling factor in Geodict. In other words, as the approach in SatuDict uses Young-Laplace equation, IFT serves only to increase or decrease the overall resulting pressure due to morphological method relying on geometrical pressure influence only. By reducing it, for instance, one will not reach smaller pores and/or change the capillary pressure curve. Therefore, it will be taken as a non-changing variable with value of 35 mN/m. This value or ones very near in range were commonly observed in the experiments, so can be taken as representative for the $scCO_2$-brine system. Examples from the literature are presented in Figure 12 and Figure 13, from the works of (Saraji et al. 2013) and (Al-Menhali and Krevor 2014), respectively.
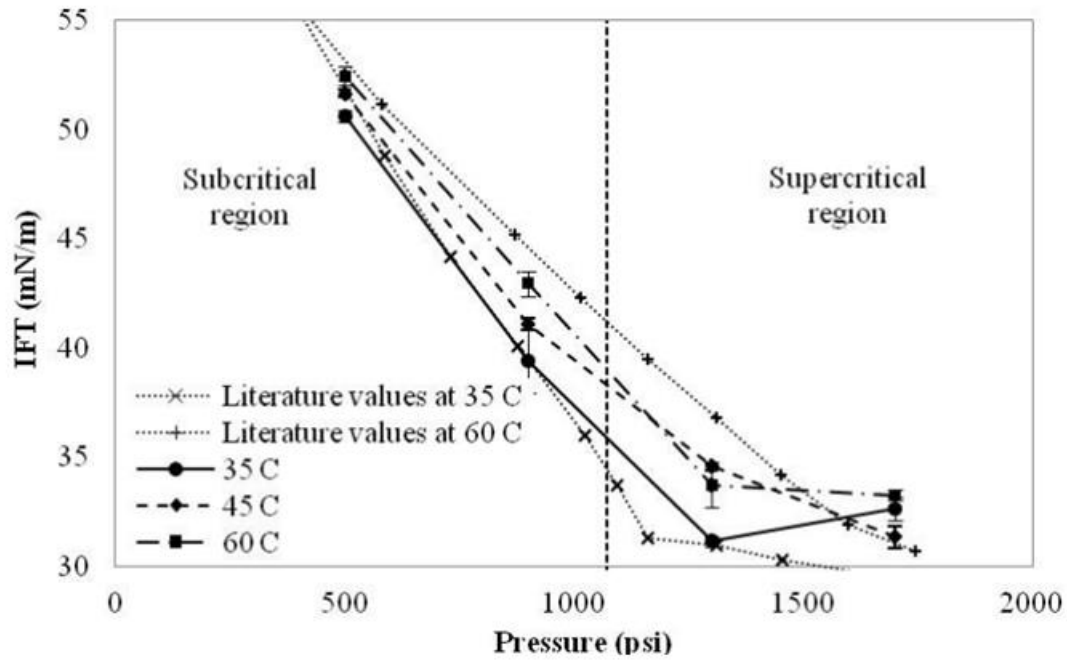
Figure 12. Comparison of Saraji and team IFT results with the literature values (Saraji et al. 2013). Values of IFT in supercritical region, as can be seen, mainly range from 30-35 mN/m.
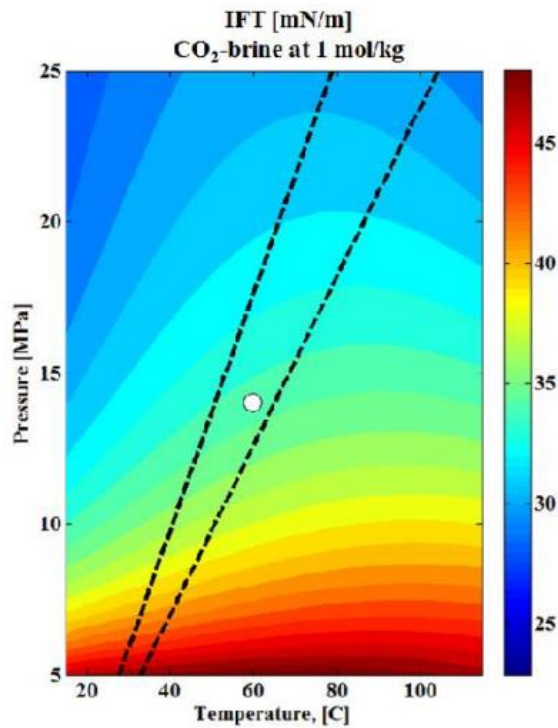
Figure 13. From (Al-Menhali and Krevor 2014). White dot are conditions used by authors, whereas the plot itself represents the range of IFT values for CO2-brine system, from (Li et al. 2012).

Land-model constants

As was previously elaborated, Land model yields the empirical relationship between the trapped (residual) NWP and its initial saturation in the rock. If wetting conditions don't change, this relationship should remain constant for a certain rock sample. By screening through various datasets from different authors, it is possible to gather significant trends for various rock samples. It can be concluded that for water-wet samples, constant will be lower compared to intermediate/oil-wet samples. The results from literature presented in Figure 14 will be used as a guideline in analysing the results obtained in this study.
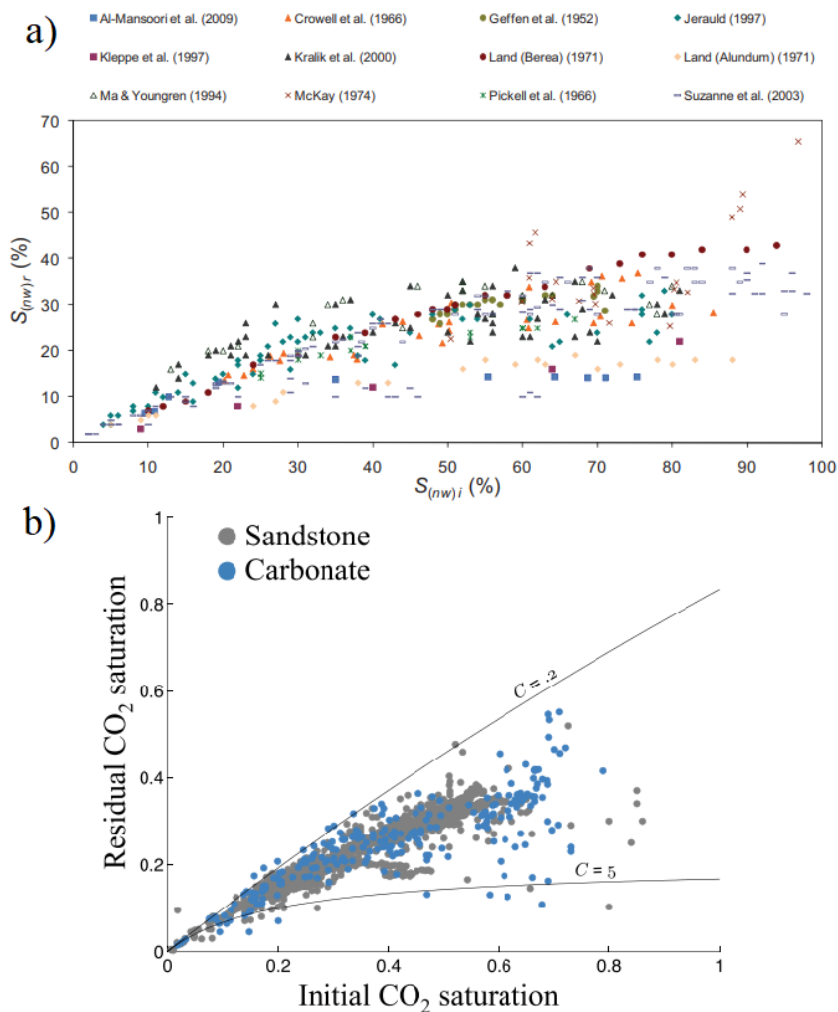
Figure 14. Experimental results from literature of residual to initial: a) NWP saturation, from (Pentland et al. 2010); b) CO_2 saturation, with sandstone and carbonate results separated by colour. From (Krevor et al. 2015). Notice the comparable trend between two plots, where first one also includes experiments with different OW phases, most commonly different oil substitutes or gases.

The observed constants range from 0.2 for highly water-wet, sandstone samples up to 5+ for oil-wet carbonate rocks. This implies a significant width of range, resulting out of rocks' heterogeneity and different wetting conditions. This large degree of heterogeneity is related to

carbonates mainly, and the rocks used in this study are sandstone representatives. That makes the comparison between this study more valid with sandstone range only ($0.7<C<2$); however, there is the connection between full range of Land-parameters and this study. It can be concluded that even for wide degree of variability of rock properties, a range of Land-model parameters should stay from 0 to 6. Based on intrinsic properties of rocks used in this study, one would expect the range in this study to be narrower – displaying more homogeneous properties. This will be discussed in next chapters, where the digital rocks used in this study and the workflow are presented.

Chapter 3

Input data & Workflow

The main goal of this thesis is to investigate the applicability of digital rock computing for simulation of trapping potentials of different digital rocks. It is of major interest fur future applicability in screening of potential CCS reservoirs. Figure 15 shows the workflow with the varying parameters. Investigations include different digital rock samples, with aim of observing the capillary trapping behaviour in different rock structures and pore geometries. Capillary trapping is described in terms of capillary pressure curves and their corresponding Land-model fits. As capillary trapping of NWP occurs during the imbibement of WP, it is necessary to carefully consider the simulation process of water imbibition and describe it in physical terms. In the software used in this thesis, simulation of imbibition is possible with two approaches. One approach involves only the process of spontaneous imbibition, and other includes both spontaneous and forced imbibition. Each of the approaches includes certain limitation that will be discussed. Additionally, within each approach, uncertainty modelling is done with aim of representing the varying rock wettability conditions.
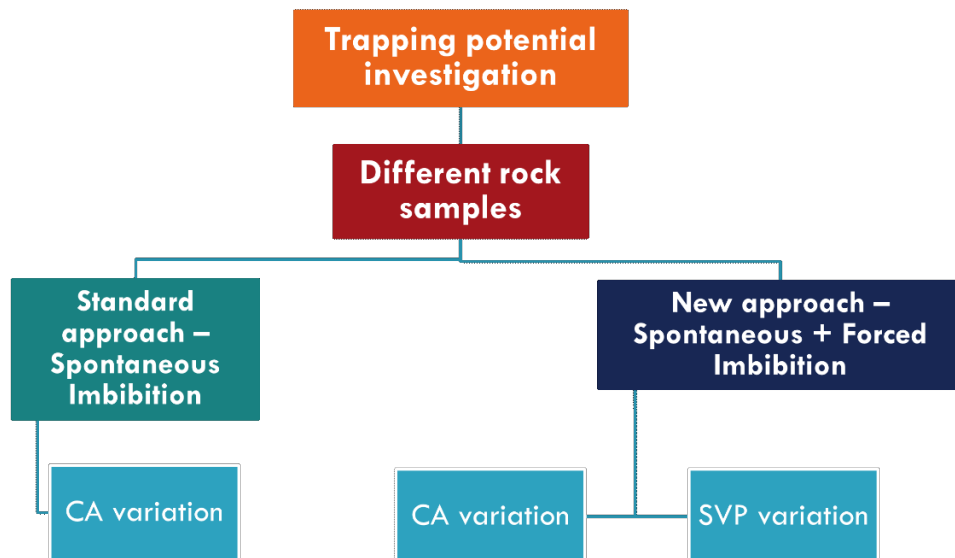
Figure 15. The decision tree with a general overview of applied workflow.

Finally, literature data is used as a reference and a quality check of data in this study.

3.1　Input Data

The input data includes six digital rock samples. They were provided by the chair of Reservoir Engineering at Montanuniversität Leoben. Samples were taken from different sandstone formations and reservoirs with differing rock properties, such as porosity, permeability, and pore size distribution. Therefore, the premise is to expect different capillary trapping. Digital rock samples are represented in Figure 16, and here are named from Sand_1 to Sand_6, including a Berea digital sample. Berea serves as a direct comparison with literature studies as it is typically used as a reference rock due to its homogeneous properties.
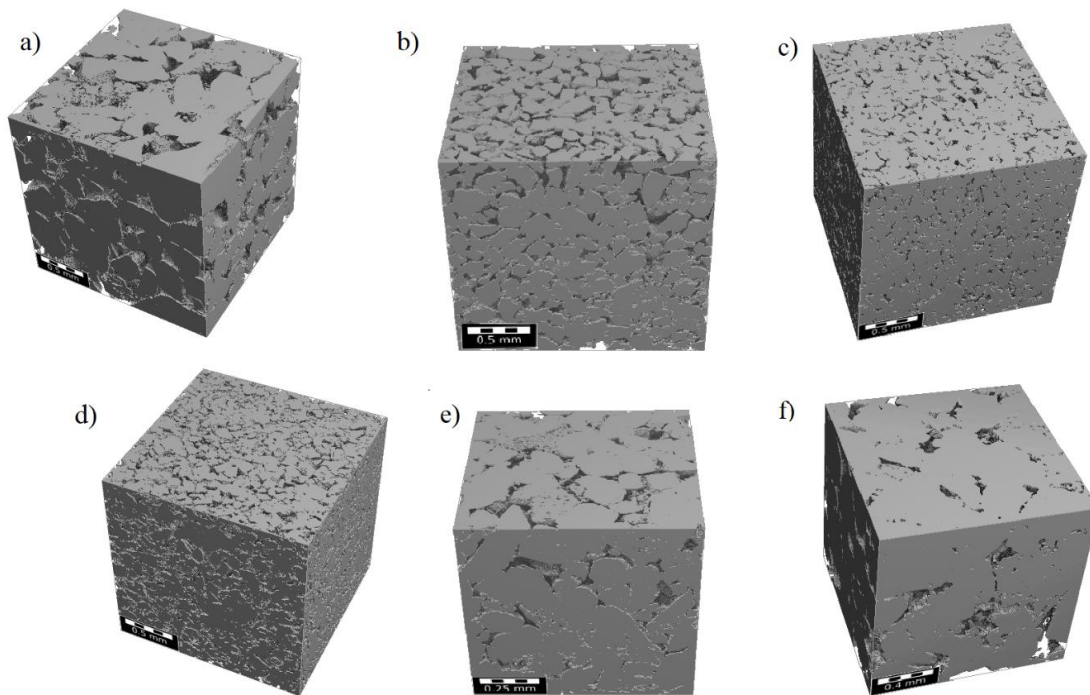
Figure 16. Five rock samples used in this study. From top, left to right: a) Sand_1, b) Sand_2, c) Sand_3, d) Sand_4 e) Berea　f) Sand_6.

The dimensions of each sample are 500x500x500 voxels. Their voxel size and porosity are listed in Table 1.

	Sand_1	Sand_2	Sand_3	Sand_4	Berea	Sand_6
Voxel size, 10^{-6} m	3.82	3.61	3.89	3.68	1.84	2.95
Porosity, %	26.3	28.3	18.7	31.8	18.3	15.9

Table 1. Voxel size and porosity of used digital rock samples.

3.2   Methodology

First in the workflow description, the fundamentals of the computational environment are briefly explained. They are needed to assure the readers' familiarity with the software and how the calculations are tackled. Next, the two imbibition approaches to create the capillary pressure curves are described, with their specialties and considerations for implementation in the existing software. The added implementation to create the trapping curves is then explained. Proposed comparison approach with the experimental database is briefly elaborated. Finally, additional parameters that allow for a statistical data analysis are considered as well.

3.2.1   Computational Environment

To conduct the simulations in this thesis, Geodict is used. It is a software used in multi-scale 3D image processing; recreating the digital material of new or existing real materials, and it is especially suitable in simulating processes in porous media, such as the ones of oil & gas interest (Planas 2021.). It has so far proven its applicability for the scientific studies of porous media in (Alexandru-Mihai Badescu 2020) and (Mario Stefan Dragovits 2021).

Geodict consists of multiple modules. The SatuDict module is of particular importance, as it is used to derive the capillary pressure curves which, consequently, yield the desired trapping curves. SatuDict's working principles are based on the updated morphological approach from (Hilpert and Miller 2001), as discussed previously in the Literature Review. As was mentioned, this approach solves the fluids' distribution according to the Young-Laplace equation expressed in radius terms, increasing the invading voxel radius from one simulation step to another and consequently changing the saturation-pressure step. This ultimately relies on the utilized structure's pore distribution. For more about the principles behind the general SatuDict functionalities and more about the Forced Imbibition tool that is used, please refer to (Math2Market GmbH et al. 2020; Mario Stefan Dragovits 2021).

In Geodict Satudict module, there are two different approaches to create the capillary pressure curves. These approaches differ in the implementation of imbibition process, as illustrated in Figure 15. There are implications to use both of them.

For instance, certain rocks have strongly-WW properties, and are consisting of homogeneous material with uniform distribution of wettability. This would imply the application of standard approach in modelling of capillary trapping. However, standard approach in Satudict so far hasn't had the implementation for forced imbibition, which would develop the unexpected shape of imbibition curve, with considerably high residual NWP saturations.

Forced imbibition implementation, on the other hand, is a promising tool that has proven realistic behaviour in development of capillary pressure curves for conditions of varying wettability. However, it hasn't been tested so far in the direct investigation of capillary trapping. Also, this approach requires necessary modifications to the digital rock. This may ultimately lead to different rock representation, with unknowns of exact rock properties. Both of the approaches will now be described.

3.2.2 Standard approach for trapping curves

Satudict module is used in the simulation of capillary pressure hysteretic cycles and other saturation-dependent functions. Therefore, it is extensively used in this study. Initially, Satudict had only the ability to simulate two capillary pressure paths:

1. Primary drainage
2. Spontaneous imbibition.

Additionally, in this approach the simulation of imbibition scanning curves is developed, and Land trapping model fitted to obtained IR saturation pairs.

To get a clearer overview of above steps, a complete simulation process is connected with the presented workflow from the decision tree in Figure 17. All the steps are further addressed in sections below.
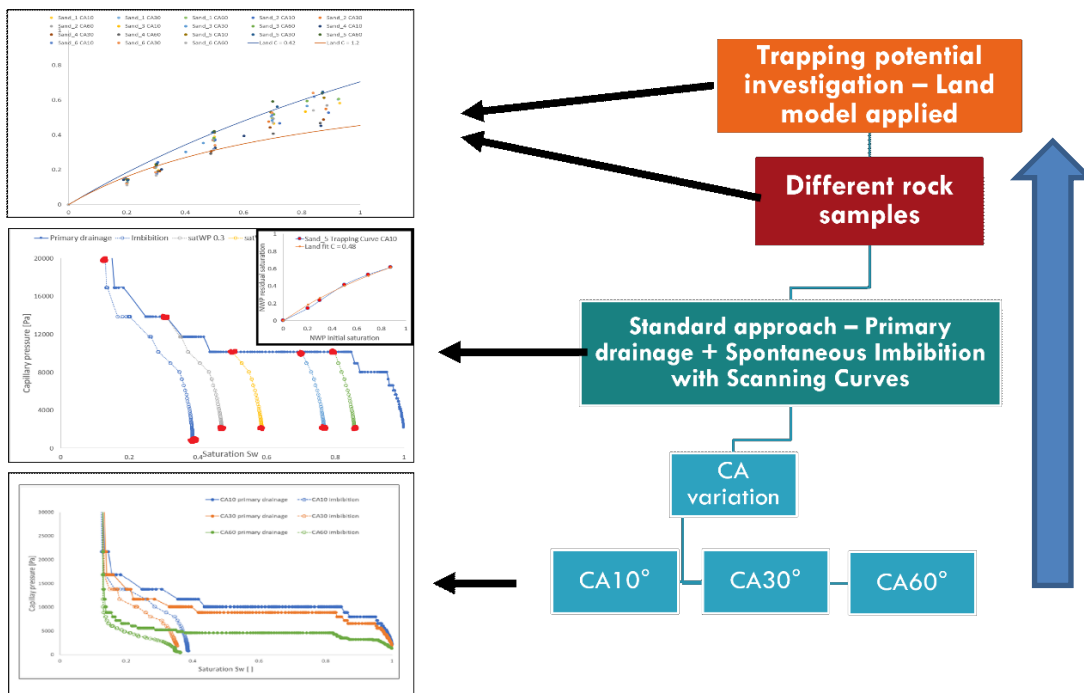
Figure 17. Overview of complete workflow for capillary trapping investigation with standard approach.

3.2.2.1 Simulation of primary drainage and spontaneous imbibition

To start the simulations, user-defined input parameters include the type of experiment (drainage or imbibition), rock material CA, IFT, and boundary conditions. Default simulation sides are used. Digital rock is initially (primary drainage) surrounded by WP reservoir at all sides but Z+, where the NWP reservoir is. This is later reversed as a part of forced imbibition macro. The property of most importance is rock material contact angle. Reason so is that it has a significant effect on the fluid phase distribution, in accordance with the YP equation, as discussed in Literature Review. Usually, higher the contact angle, the rock is more NW, and thus yields the lower total NWP residual after the full imbibition. However, within the standard approach, the premise is that higher CA will lead to earlier zero-crossing of capillary pressure, thus reaching the higher NWP residual after the spontaneous imbibition.

Sensitivity analysis of CA is done with CA of 10°, 30°, and 60°. With each CA, capillary pressure curves were created. Both primary drainage and spontaneous imbibition would be affected by CA variation, and one such example is given for Berea sample in Figure 18.
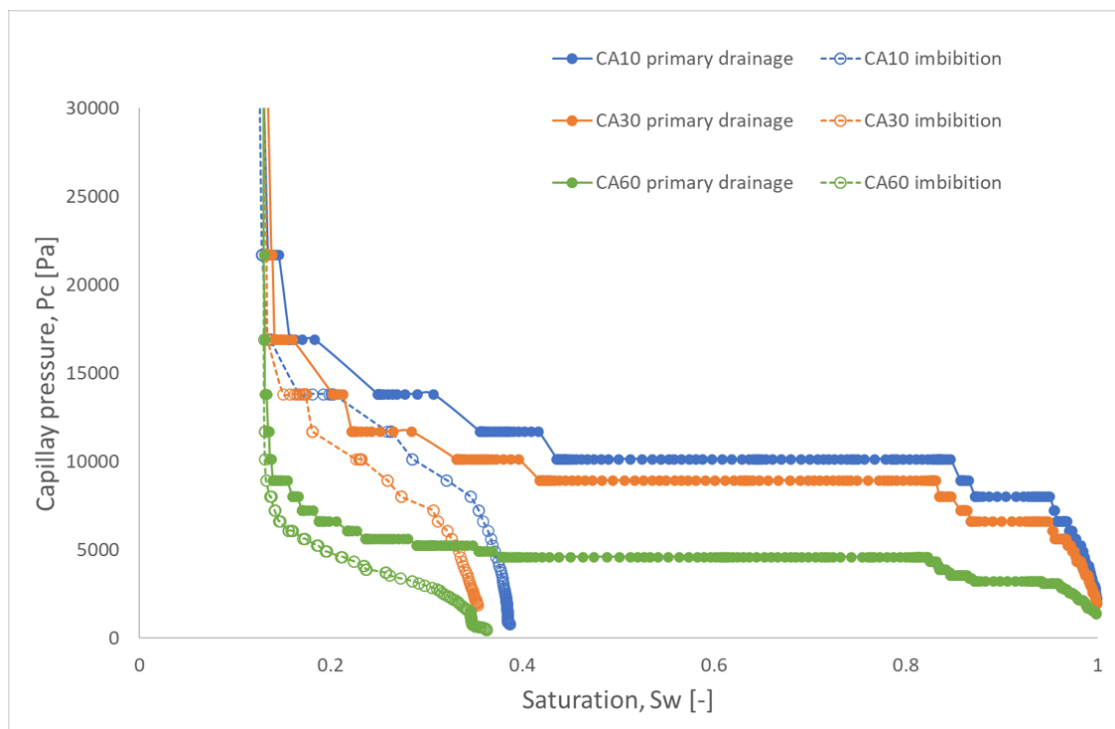
Figure 18. Berea: Illustration of the influence of different CA applied to rock material on the capillary pressure curves.

Notice the influence of CA. Trend in primary drainage shows higher plateau with larger CA value, which is in accordance with realistic observations. The irreducible water saturation is approximately same for all contact angles, while there are minor differences in residual NWP saturation. Here it has to be mentioned that simulations ultimately don't end at exact pressure steps. This is due to the calculating approach of pore morphology method (PMM) and numerical

artifacts that arise at larger dilation steps combined with the CA implementation. However, this effect is observed as minor and ultimately not making a substantial impact on residual saturation reached. For more details, please refer to (Schulz et al. 2015).The effect of CA on residual NWP saturation is of main interest, as capillary trapping models rely on initial-residual NWP saturation pairs.

3.2.2.2 Development of imbibition scanning curves and Land model fitting

After simulating primary drainage and imbibition, next step is to develop the implementation to simulate the imbibition scanning curves. They are imbibition paths starting at turning saturation points on the drainage curve, earlier than reaching the irreducible WP saturation. Geodict by default doesn't offer this functionality and it was implemented with simple scripting. Script code revolves around loading the structure from drainage simulation at the wanted turning saturation step, reading the diameter voxel size at that step, and applying it as the initial step size for dilation in imbibition process. Illustration of Berea results at a turning saturation step of 0.3 is given in Figure 19, right before the imbibition process.
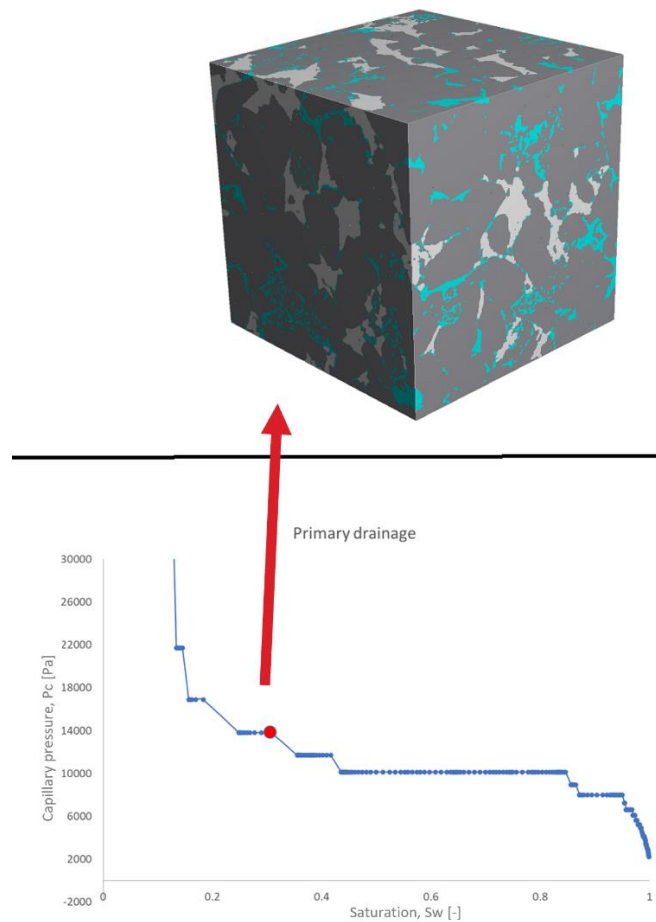
Figure 19. Illustration of rock cube at a turning saturation step Sw = 0.3. Drainage state at a given saturation will be loaded, and imbibition process started. Dark grey: rock solid; cyan: WP (brine); light grey: NWP (CO$_2$).

The turning saturation points can be user-defined, and here include a range from WP saturation of 0.3 to 0.8. The script developed in this study reads out reached saturations for every simulation step. The simulation step that has saturation closest to turning saturation from above range is then loaded, and used for further imbibition simulation, which then runs until the residual NWP saturation is reached. Illustration of rock structure with different residual NWP saturations reached is given in Figure 20. The rock structure is illustrated during the primary imbibition and for middle case of turning WP saturation of 0.5 and low-case of turning WP saturation of 0.8.
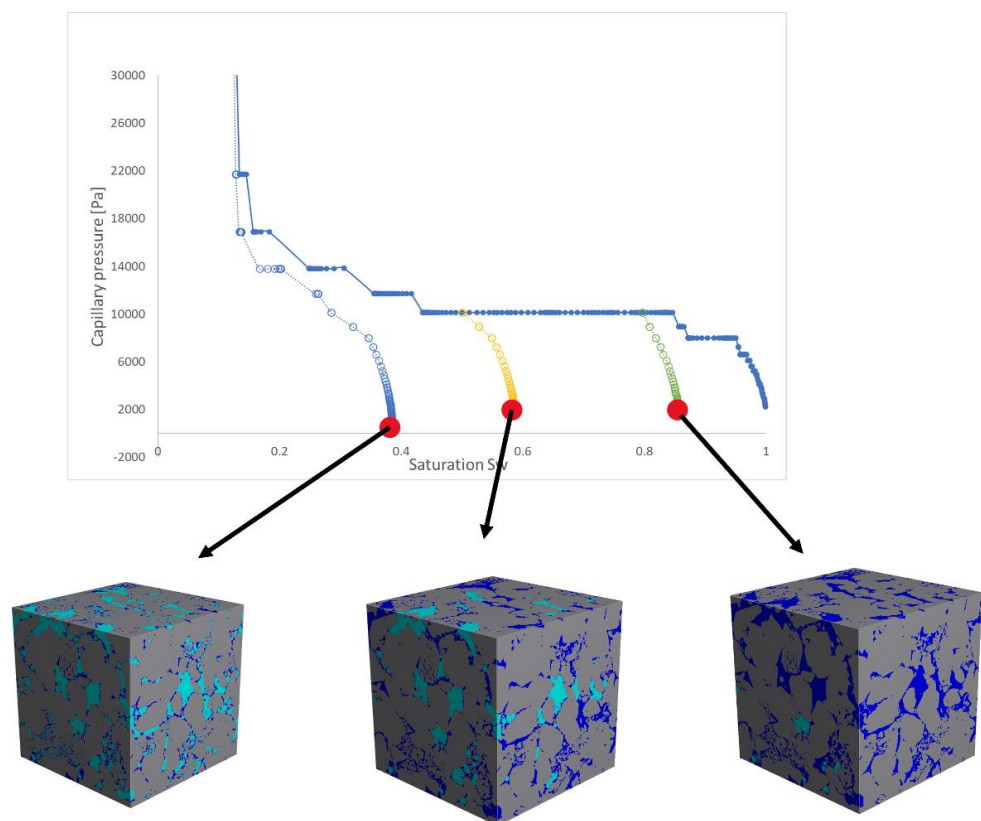
Figure 20. Illustration of different residual NWP saturations reached with different imbibition scanning curves. From left to right, rock structures are after: primary imbibition; turning WP saturation of 0.5; and turning WP saturation of 0.8. Grey: rock solid; cyan: NWP (CO_2); dark blue: WP (brine).

Scanning curves are crucial for fitting the capillary pressure data to trapping potential with application of Land model. Such a fit is illustrated in Figure 21.
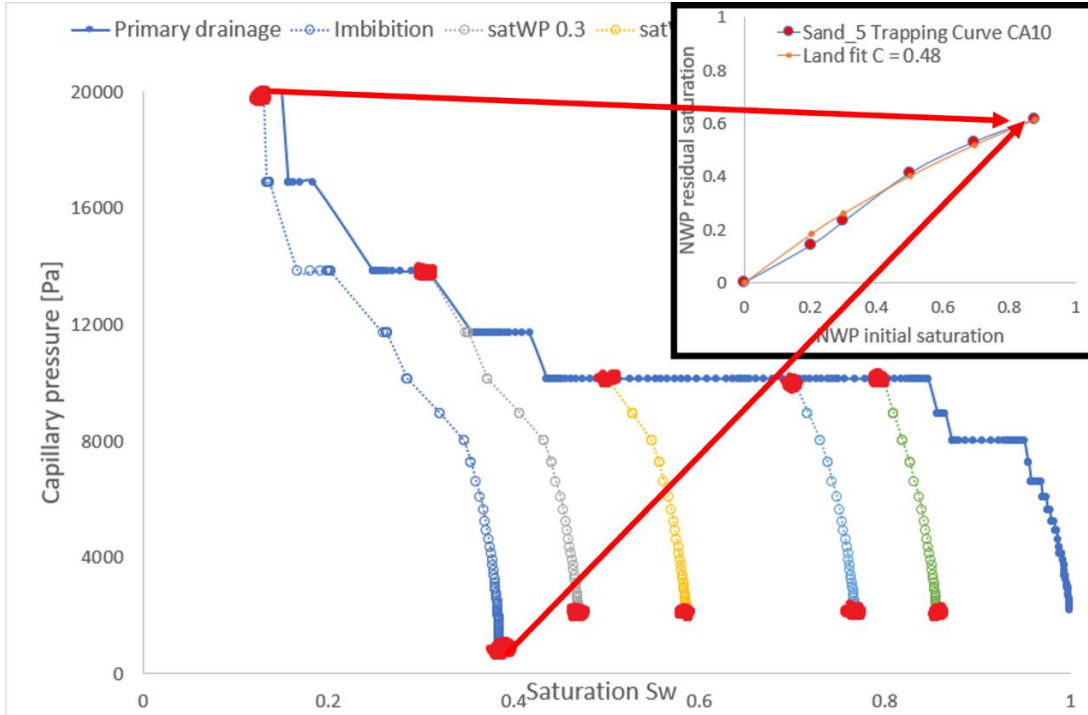
Figure 21. Illustration of simulated imbibition scanning curves, and the respective Land model fit in small plot. Initial-residual saturation pairs are marked in red.

Initial-residual NWP saturation pairs are marked in red, and Land model is fitted to them with following equation by changing C value:

$$S^*_{NWP}, r = \frac{S^*_{NWP}, i}{1 + CS^*_{NWP}, i}$$

where $S_{NWP, r}$ is residual NWP saturation reached in imbibition, $S_{NWP, i}$ is initial NWP saturation reached during primary drainage, and C is Land-model parameter that is directly connected to intrinsic rock properties and its wettability. Same procedure is repeated for all CA cases, resulting in 3 trapping curves per digital rock, and 18 in total. They will be presented and discussed in the Results section.

Developed trapping curves are then compared with the literature as a quality check on obtained results. As the literature range with Berea sample includes C values from 0.7 to 2, it may be considered that trapping results in this study should be near or within the literature range. However, differences between simulation procedure/results and literature have to be addressed.

48

3.2.3 New approach for trapping curves with Forced Imbibition

Second approach in this thesis focuses on development of trapping curves with the forced imbibition tool, recently implemented in Geodict. Its performance and physical representation of saturation dependent processes were confirmed in study by (Mario Stefan Dragovits 2021). Newly developed workflow is shown in Figure 22, and sequentially it includes:

1. Adjustment of the digital rock structure with the varying CA and SVP
2. Primary drainage
3. Spontaneous and forced imbibition (full imbibition branch)
4. Scanning curves for full imbibition branch
5. Fitting of Land model.
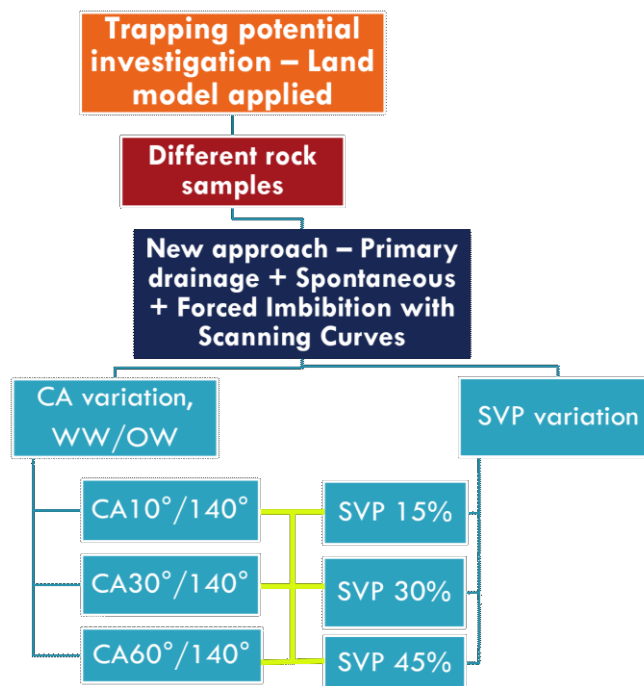
Figure 22. Workflow overview with the implementation of forced imbibition.

3.2.3.1 Rock structure adjustment

To implement the forced imbibition, NW material is needed, which is implemented by adjusting the rock structure. Rock structure has to consist of at least two rock materials. One has to be WW, and other has to be NW, or precisely, having the wettability over 90°. This requirement is due to the calculation principles of forced imbibition tool that aim to mimic experimental conditions. Namely, forced imbibition is modelled as drainage from the previously-set WP reservoir. For more details about the overall process of forced imbibition setup, please refer to (Mario Stefan Dragovits 2021).

First, NW material is assigned to the rock structure. Throughout this thesis it is referred to as Solid Volume Percentage (SVP), which indicates the percentage of rock structure changed to NW conditions. To apply the secondary material, Distribute Contact Angles (DCA) macro was used. It is part of the forced imbibition tool. This approach distributes NW material statistically throughout the initial rock structure, as can be seen in Figure 23.
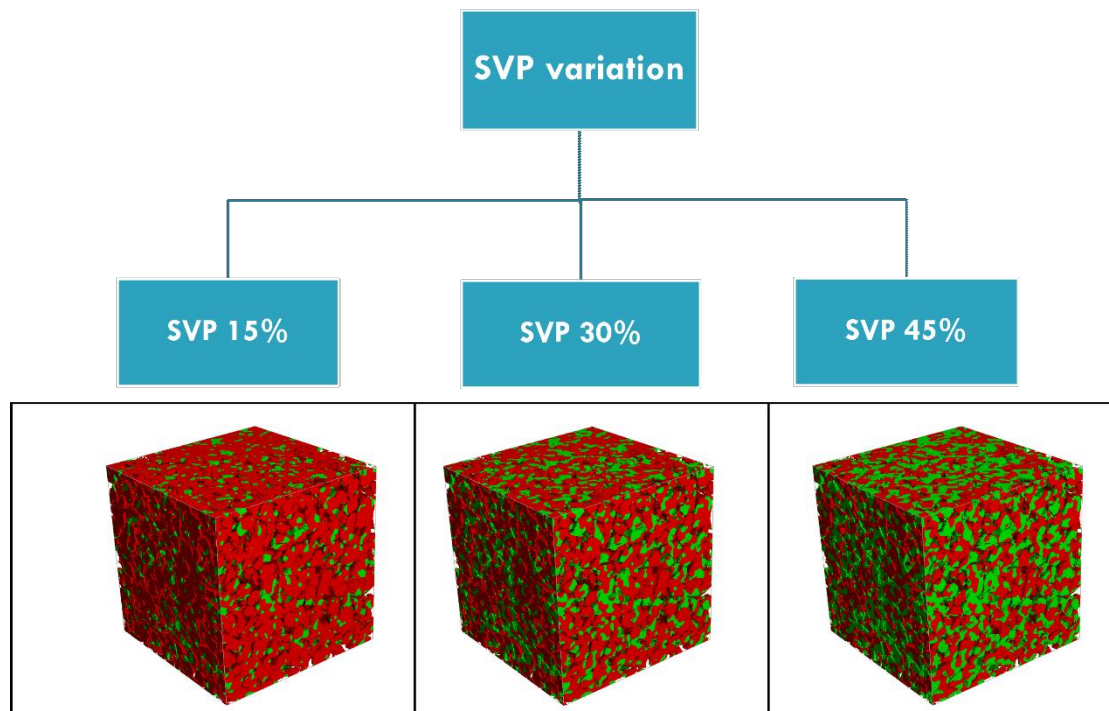
Figure 23. Statistical distribution of secondary material expressed with SVP increase. Initial rock material is red, and secondary NW material, varied by SVP %, is green.

As CO_2 is virtually never a wetting phase in reservoir conditions, this approach focuses on statistical distribution of secondary NW material rather than implementing it with TORS functionality, as in (Mario Stefan Dragovits 2021). TORS would change the material in contact with the pore space reached by NWP. This would alter the wettability similarly like the process of wettability change in oil reservoirs. Also, TORS has shown higher impact on the residual NWP saturations than SVP implementation. In this study the focus is on sandstone samples of initially high WW. Therefore, only the necessary adaptation of secondary material with SVP is done to implement forced imbibition. This implementation also impacts the drainage part of capillary curve, as it is done before any simulation. Important to mention is that by this approach surface area is directly related to volume of secondary material, which plays a role as determining the amount of contact between fluid in pores and the material of certain CA.

Then, 3 contact angle pairs are chosen for the sensitivity analysis. Combining 3 CA pairs with 3 different distributions of SVP results in 9 total cases per sample illustrated in Figure 22 and Table 2. Initially, plan was to develop 9 different trapping scenarios. However, with CA 60°/140° pair, the variation in capillary pressure curve and subsequent trapping is minimum, which is seen in Figure 24 and will be discussed. To reduce the redundancy, only the middle case of CA60_SVP30 will be developed into trapping curves.

Table 2. Different scenarios for simulation of capillary pressure curves. 9 per sample, 63 in total.

Case Nr.	CA WW	CA NW	SVP, %
Case 1	10°	140°	SVP 15%
Case 2	10°	140°	SVP 30%
Case 3	10°	140°	SVP 45%
Case 4	30°	140°	SVP 15%
Case 5	30°	140°	SVP 30%
Case 6	30°	140°	SVP 45%
Case 7	60°	140°	SVP 15%
Case 8	60°	140°	SVP 30%
Case 9	60°	140°	SVP 45%

Additional sensitivity analyses in this and previous studies have shown that most of the influence is delivered by WW CA alteration, whereas NW CA makes minor influence. Therefore, NW CA isn't altered throughout the main investigation and will be left out of further naming convention for simplicity.

3.2.3.2 Capillary pressure curves with Forced imbibition

After setting up the simulation rock structure according to above procedure, drainage and imbibition can be simulated. 9 different capillary pressure curves are developed per sample. Illustration of combined CA-SVP effect on capillary pressure curve is given in Figure 24.
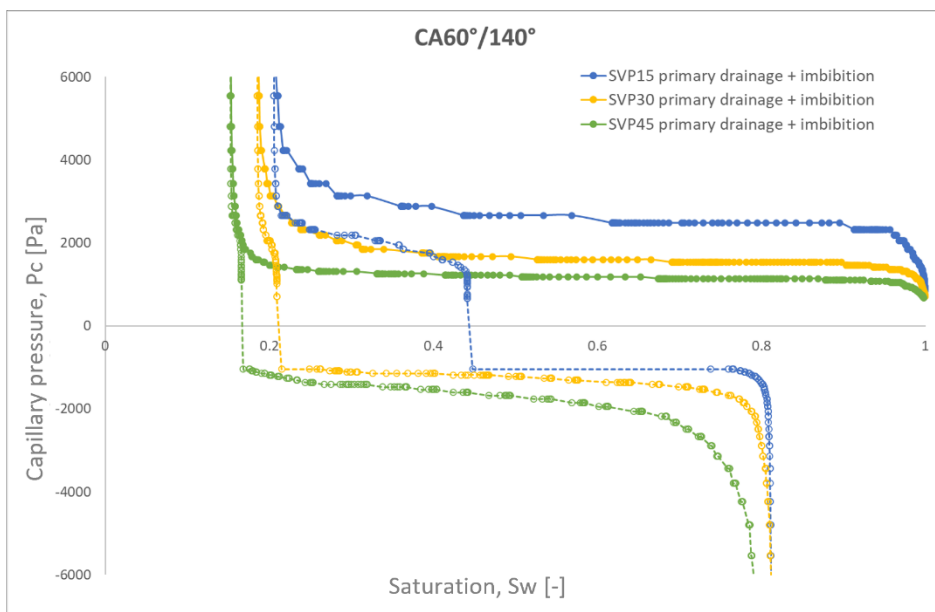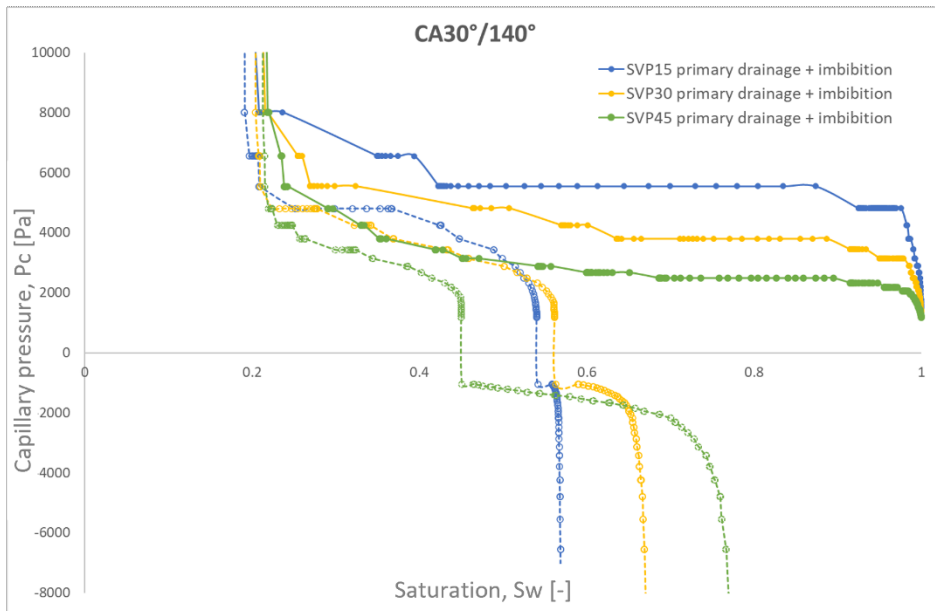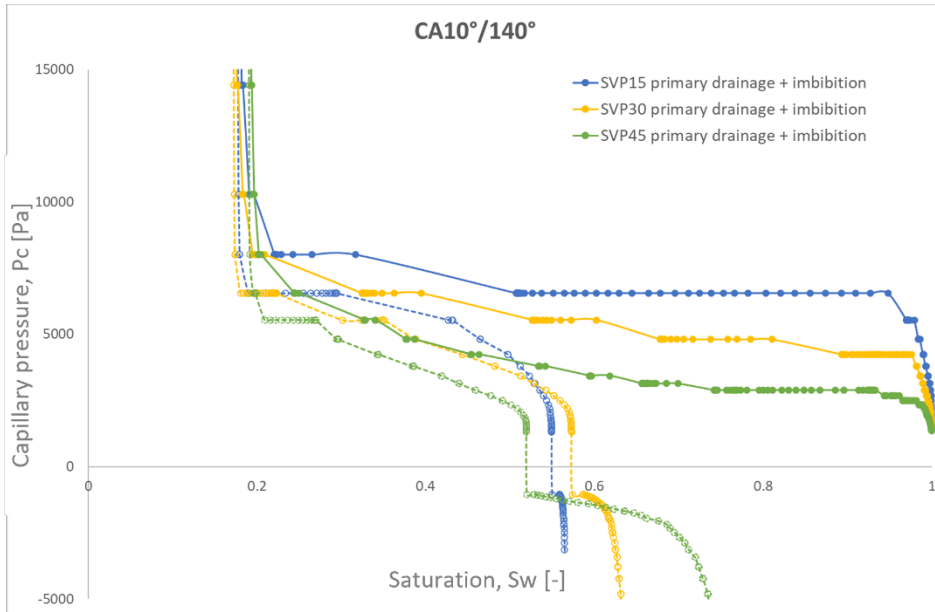
Figure 24. Illustration of obtained capillary pressure curves from 9 combined cases. Notice the considerable effect on NWP residual saturation within CA10/140 and CA30/140 comparisons, and minor impact for CA60/140 case.

Observed trends are in line with wettability shifts and they are a part of confirmation of results in previous study by (Mario Stefan Dragovits 2021). Increased contact angle results in lower pressure plateau during drainage, earlier zero-crossing, and lower residual NWP saturation (main interest of this study). Also, increased volume of NW material moves the overall wettability in correct direction, showing considerable effect on the capillary pressure curve. This is the basis for application in capillary pressure and trapping potential investigation.

3.2.3.3 Scanning curves for full imbibition range

As a next step, scanning imbibition curves are developed for each of the cases per each rock sample. Only exception are the cases for CA60°/140° pair. As observed in Figure 24, CA60°/140° pairs are not suitable for trapping potential investigation as the residual saturation does not vary with SVP variation. This happens due to CA60° being near the numerical error boundary, as the morphological approach cannot handle mixed-wet conditions (near CA90°). Therefore, only one case, namely CA60°/140° SVP30, will be presented with the developed trapping curves.

Land model is fitted to scanning imbibition curves in the same fashion as in Standard approach, described in above section 3.2.2.2. Fit is illustrated in Figure 25.
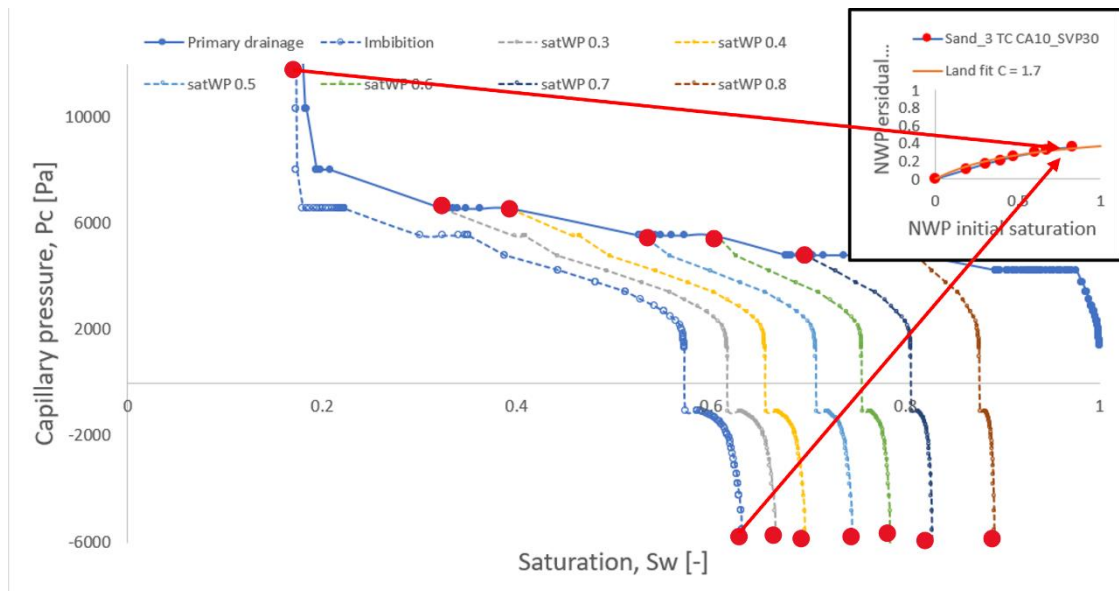
Figure 25. Illustration of simulated imbibition scanning curves, and the respective Land model fit in small plot. Imbibition includes the full range, spontaneous and forced. Initial-residual saturation pairs are marked in red.

3.2.4 Additional investigations and evaluation of petrophysical properties

Capillary trapping potential is evaluated for different rock structures across a wide range of mentioned parameters. The results of both approaches are presented and analysed in the next Chapter. Further investigation of capillary trapping is then focused to resolve the observed trends and to check whether they are similar to those observed in the literature. For instance, there are unclear IR saturation pathways at early turning-saturations, showing mismatches with the Land-model. Such trends may arise from end-effects at the boundaries of the structure. The imbibition process modelling in GeoDict requires the respective phases to be connected to their reservoir (boundary), otherwise no displacement events can happen. Therefore, the spontaneous and/or forced imbibition can be halted prematurely. This effect may in particular be observed at earlier simulation steps, yielding the large discrepancy between simulated results and Land model. To further investigate the influence of the capillary end effects, simulations were done on extended domain. The extension of the domain size is modelled by mirroring the structure in Z-direction, which is used as the axis of inlet and outlet during simulations. This enlarges the domain only in Z-direction, while it remains of same size in x and y-directions. Then the results are observed across the whole domain, as well as at each half to see the boundary influence. Additionally, boundary end effect is supposed to be reduced by using the large domain simulation with the same assumption as with extended domain. Large domain is of size 1000^3 voxels. Comparison of three domain sizes is given in Figure 26, sketching the impact domain size may have on mitigating the boundary end effects.
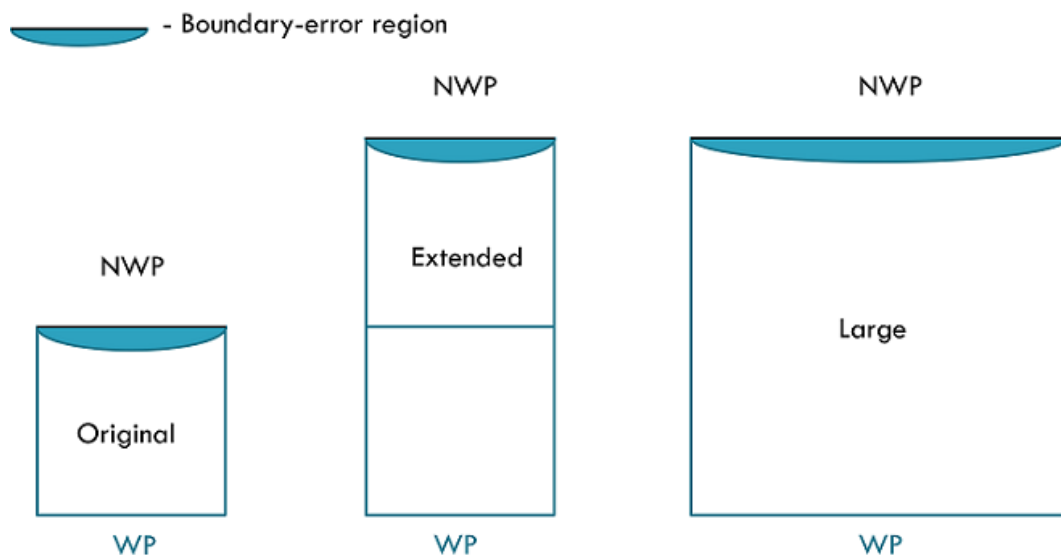
Figure 26. Boundary end effect is presumed to have the most impact on smallest domain size, as the boundary-error region is proportionally largest.

Additionally, large domain incorporates substantially more pore space, changing the pore size distribution of the structure/s. That may show considerable impact on trapping potential.

For clearer insight on trapping potential, new Berea sample is used as it is the connection between this study and literature, where the Berea was in main focus. Additionally, new Berea has voxel size that is comparable to other samples, whereas original Berea has approximately 50% smaller voxel size. This gives insight in the impact voxel size may have, and also the other structure properties.

For the most part, visual fit of Land model to IR points is providing a possibility for a qualitative comparison and ranking. However, a more precise fit is needed to exactly describe the trapping potential in terms of Land-model constant. This fit is done by applying least squares method to match Land model with simulated IR points, as in (Land 1968). Matched Land-model constants are then correlated with the structures respective petrophysical properties, including porosity, permeability, coordination number, pore throat and pore size distribution, and pore to pore throat aspect ratio. To compute the petrophysical properties the module PoroDict, in particular Identify Pores, Granulometry and Porosimetry, is used. For more details on PoroDict and its functionalities, please refer to (Math2Market GmbH et al. 2020). All analyses are performed while ignoring pores at the domain boundary.

The coordination number is representing the number of connections a single pore has. As the structures consist of hundreds of thousands of pores, the average value is calculated. It directly represents how many pathways a phase can take during intrusion. The intrusion pathway is then based on the capillary pressure and consequently the pore throat size, which is next property of interest. The pore throat size distribution is obtained with Porosimetry functionality that mimics MICP. The focus in porosimetry is on accessible pore volume, and same approach is used as in drainage modelling within morphological method. Next property is the pore size distribution, obtained with Granulometry functionality within PoroDict. This functionality inscribes spherical shapes in pore space to determine the pore sizes. It also includes closed pores, not accessible to flow and capillary trapping. Two pore size distributions precisely show the sizes of pores and throats, which are crucial in capillary trapping processes. They are here presented with characteristic diameters at distribution ranges. For instance, D10 is the diameter size that is larger than 10% of all pore diameters, or vice-versa, smaller than 90% of pore diameters, and D50 and D90 diameters follow. These values are here focused, as they are easily relatable with respective Land constants, opposed to distribution functions. Finally, the ratio between pore body and pore throat yields the pore aspect ratio. Aspect ratio is considered crucial in capillary trapping processes, therefore its correlation with trapping could potentially identify significant trends. However, this parameter cannot be directly calculated in Geodict. As an estimation, statistically-calculated aspect ratio is derived from pore body to pore size characteristic

diameters at earlier specified distributions. Its value however may not indicate the most appropriate description of aspect ratio and therefore has to be acknowledged as an estimation at statistical ranges.

For a clearer insight, all correlations are illustrated along the Land parameters and further discussed.

Chapter 4

Results and Discussion

In this section, results from Standard and New approach for development of trapping curves are presented and discussed.

First, all the simulated cases for each of the approaches are presented. Then, their significance in relation to CA – standard approach – and CA/SVP – new approach with FI – is discussed and further illustrated. Further data analysis includes sample-to-sample relative comparison. Additional investigations of Berea on a larger simulation domain and another Berea sample are parts of domain-size investigation, and a qualitative comparison to experimental database previously mentioned, as Berea is the direct connection between this and other studies. Evaluation of rocks' pore geometries relationship to capillary trapping is the next step. This includes different statistical and petrophysical parameters described in section 3.2.4.

4.1   Trapping curves with Standard approach – SI only

Trapping curves developed with the standard approach are shown in Figure 27. They include three CA variations per rock sample, for six different digital rock structures, totalling 18 curves. At early turning saturation points, Land model doesn't match with simulated initial-residual saturation pairs. The trend of simulated results along whole saturation range can be considered linear. Land model fit, on the other hand, generally exhibits asymptotic behaviour. This leads to mismatch that may be due to different reasons. They include inadequate fitting of the model; this however is most likely here not the reason, as the model here is fitted according to the whole range of IR pairs with least squares method. Other reasons may include inability of morphology method in description of realistic water-wet trapping conditions. Such reason may involve different aspects which require deeper investigation. Potential solutions will be tackled in later section of this study, by observing the influence of domain size and boundary end effects. Further explanation can include inadequacy of Land model for this purpose. However, the Land model was precisely developed for trapping of gas in water-wet conditions, which is also targeted here. Nevertheless, certain assumption may be considered for application of Land-model. The aim of this study is in investigation of trapping potential through means of Land-

model parameters obtained for each simulated case and rock structure, and then making a quality check comparison with literature data range observed for common sandstone structures. For that purpose, Land model is still a valid tool as it captures the trapping potential of digital rock structures, which relies on structures' geometries and wetting state. Finally, similar behaviour is seen within literature range too, where the early IR pairs can be observed out of Land model range. This may indicate the inability of Land model to completely capture the trapping behaviour, both in experiments – literature – and in numerical simulations – this study.

Upper and lower boundaries of simulated results in Figure 27 are captured with Land-model parameters of C=0.42 and C=1.2. These values indicate considerably high degree of capillary trapping for the used digital rocks, when compared to experimental data range from (Krevor et al. 2015). There, the C values that capture upper and lower boundaries for 95% of sandstone data are in range from 0.7 to 2.
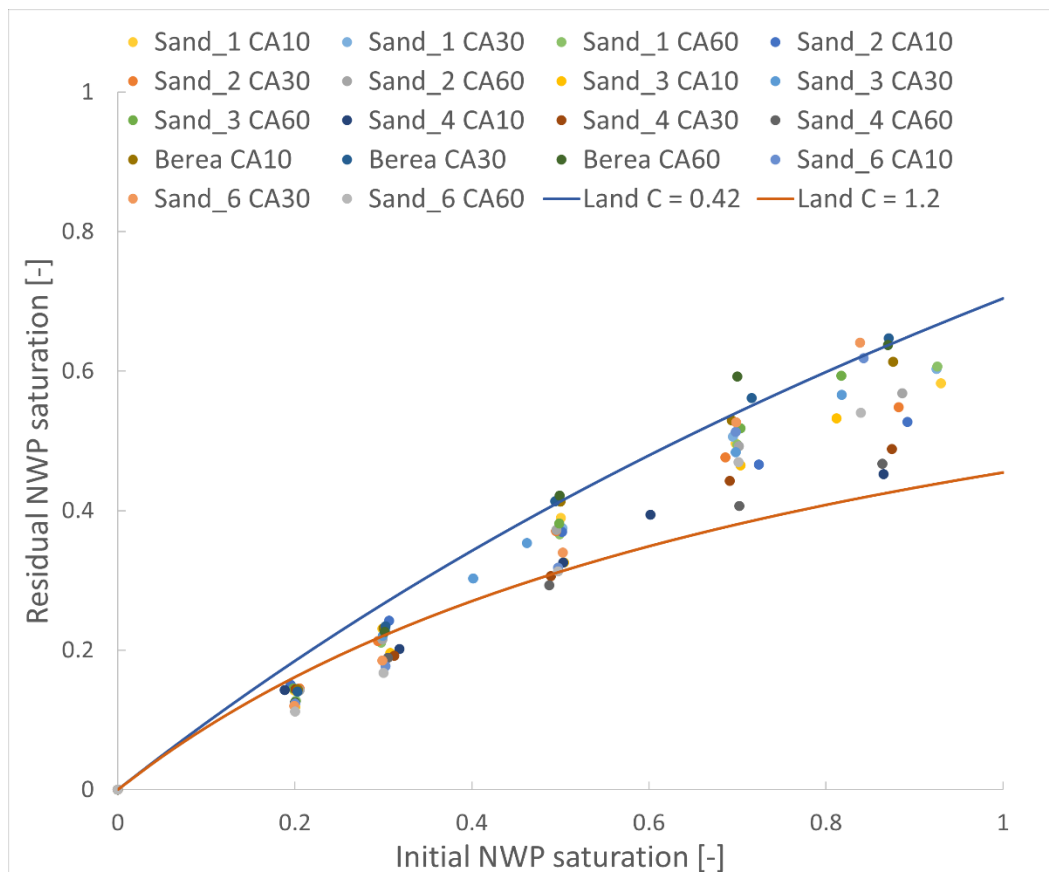
Figure 27. Trapping curves developed with standard approach (SI only), expressed as dots for all simulated cases. 3 per sample, 18 in total. Upper and lower Land-model boundaries are C = 0.42 and C = 1.2.

Same data is now expressed in form of 3 CA variations in Figure 28. As can be seen, there is no clear trend between different rock samples, once the trapping curves are grouped according

to CA. There is the unexpected degree of results' discrepancy when it comes to relationship between CA and trapping. For majority of cases presented, the capillary trapping in terms of Land curves is larger with higher CA. This is related to earlier zero-crossing, and thus earlier residual NWP saturation reached which is physically correct. However, the part not captured with Standard approach is related to forced imbibition. Namely, in experimental conditions, it is expected that rock with lower CA will have smaller change in residual NWP saturation with forced imbibition. Rock with higher CA, on the other hand, is expected to have earlier zero-crossing at larger NWP saturation, and ultimately lower residual NWP saturation with increasing forced imbibition pressure. This cannot be represented with the standard approach and thus yields unexpected trends in capillary behaviour. That is where the implementation with forced imbibition promises substantial improvement in obtained results.
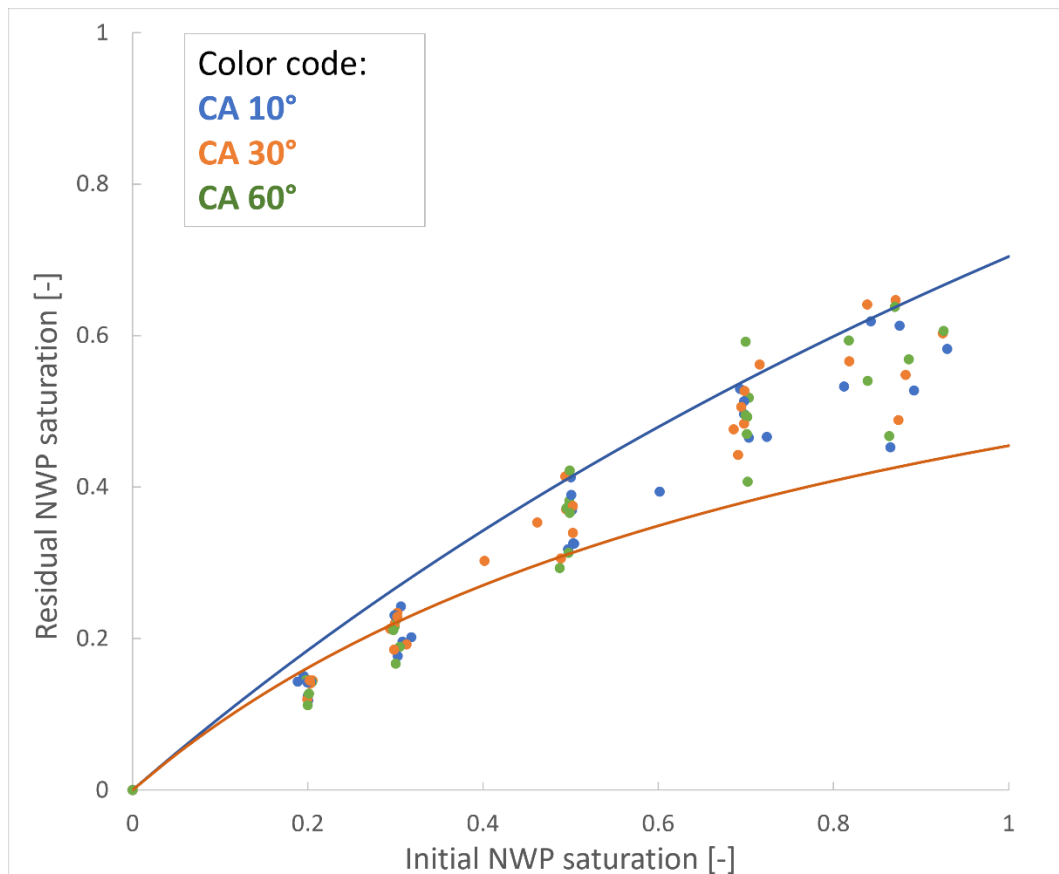
Figure 28. Trapping curves with standard approach, now classified by contact angles to see the difference between rock and CA influence. No clear trends in CA variation between different rock samples is determined visually.

Finally, data are represented on the sample-to-sample basis in Figure 29, where each sample is in a different colour. Each sample contains CA10, CA30 and CA60 case in same colour. There is the clearer distinction now, with every sample having a specific trapping curve behaviour, and uncertainty modelling incorporated with the varying contact angles. In other words, there

is no substantial variation within same sample with different contact angles implemented. Deductively, this may imply considerable effect of rock geometry that plays a role on most of the trapping potential. These correlations between various effects will later be tackled.

Next section will present the results with new approach that incorporates forced imbibition in the development of trapping curves.
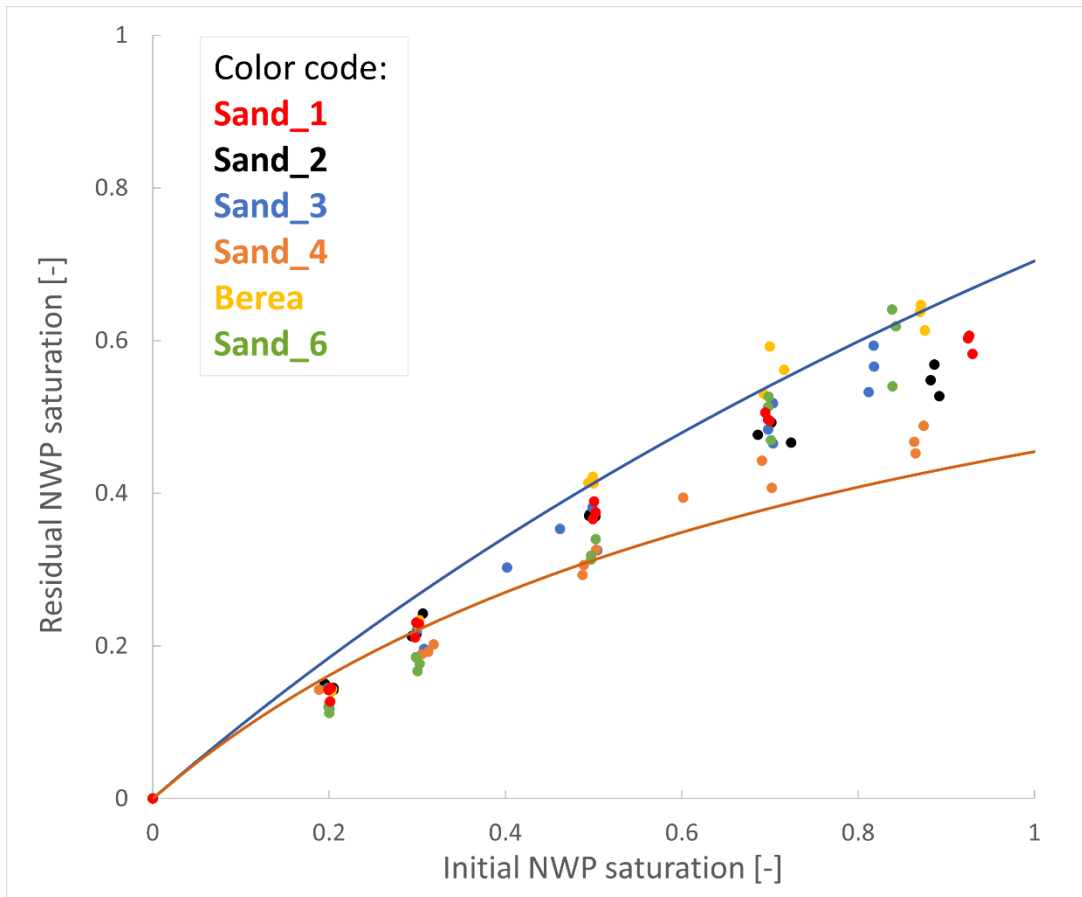
Figure 29. Trapping curves data presented in sample-by-sample basis. Notice the small degree of variation incorporated with varying contact angles, and clearer trends on a sample basis.

4.2   Trapping curves with new approach – SI + FI

Next, the process of capillary trapping investigation is extended with the implementation of forced imbibition. Simulated trapping curves are here presented for all digital rocks and cases in Figure 30.

Upper and lower boundaries are captured with Land-model parameter of C = 1.15 and C = 11. The upper boundary is in line with the mentioned experimental data range, while bottom range is significantly skewed. To get a better understanding of capillary trapping in the used digital samples, parameter-by-parameter plots will be shown next. In plot of SVP classification, there is the noticeable influence of SVP. As the SVP increases, capillary trapping decreases. As the SVP increases, there is less of variation in curves between samples. However, it has to be noted that although trapping curves are grouped at bottom, the range of C values is still from 4 to 10. This is not clearly distinguishable due to scale of Land model not behaving linearly.
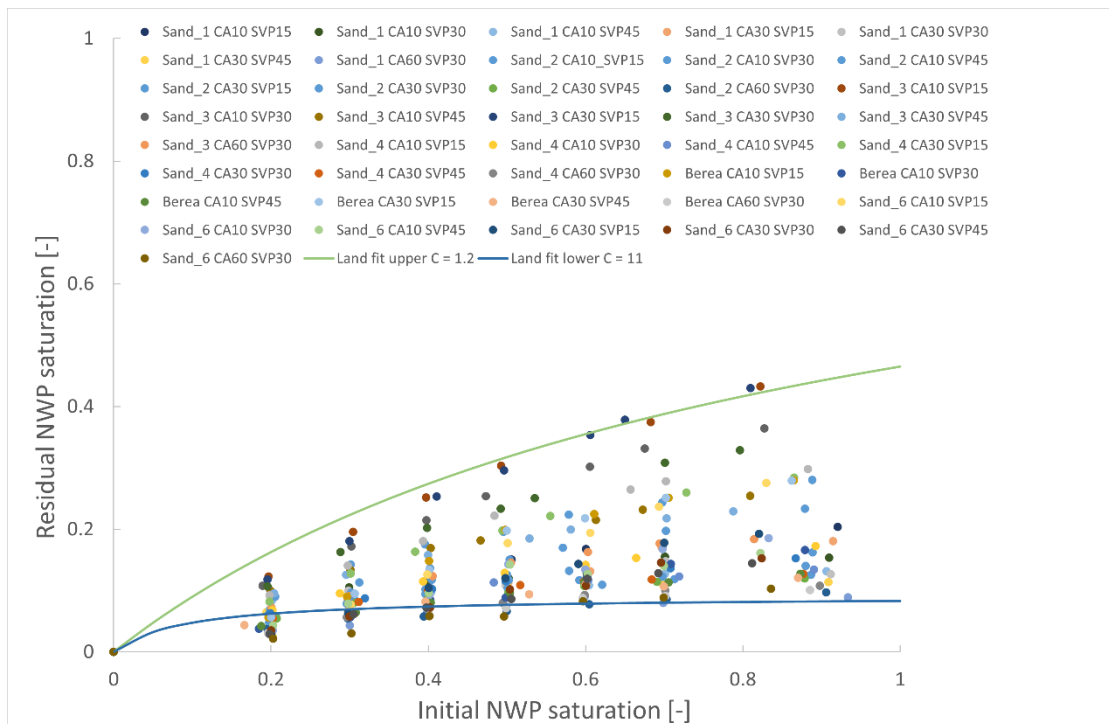
Figure 30. All simulated trapping curves with new approach that includes FI.

Trapping curves shown by SVP classification are plotted in Figure 31.
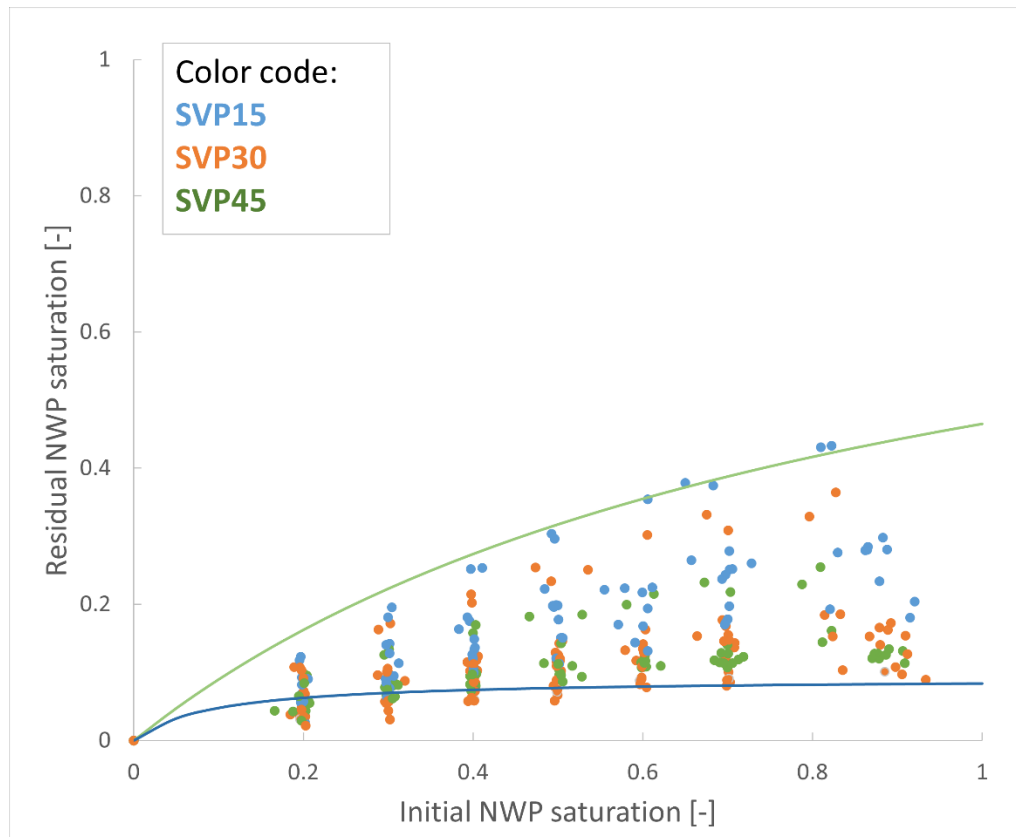
Figure 31. Trapping curves classified by SVP, across all rock samples.

Anyhow, as scale doesn't behave linearly, there is also much wider variation in trapping capabilities from C = 1 to C = 4, then from C = 4 to C = 10.

Further investigation of SVP influence will show each of the SVP-grouped trapping curves in Figure 32. Emphasizing with SVP-groups makes it evident that SVP clearly shifts the trapping behaviour and that it has an influence nonetheless of CA applied to samples or their rock geometries. Therefore, it has to be carefully considered due to the impact it has, as the shown behaviour indicates potential dominance of SVP value on the wettability and overall trapping capabilities. One suggestion, if this workflow is applied for screening of water-wet reservoirs for CCS, is to not use the SVP values over 30%.

Next investigation tackles the influence of CA variation. Without forced imbibition, results show inconsistency of CA influence, and it is presumed that its effect would now be more exhibited.

Figure 33 shows the grouping of samples according to CA. Here, no clear distinction between CA10°/140° and CA30°/140° is seen. There is considerable overlap in curves between these two cases, thus implying inconsistent trend due to CA. As SVP has previously shown large influence, its combination with CA is most likely to have larger influence on trapping curves than CA on its own.

CA60°/140° case, on the other hand, shows considerable downtrend with minimum trapping exhibited. This clearer distinction with CA60°/140° is probably due to the significant shift in wetting conditions towards oil wettability. Now, rock can virtually be considered as mixed to oil-wet and there is no more WW behaviour at all. Also, these values may be in range of numerical instabilities within the calculating algorithm; thus, showing smaller variation in trapping behaviour.

In either case, suggestion is that CA60°/140° is skewing the wetting too negatively for application of this workflow to water-wet reservoir rocks. Based on previous consideration not to use SVP over 30% and this one regarding CA60°/140°, it is suggested to use maximum of contact angle pairs 10°/140° and 30°/140° and maximum SVP 30%. These cases are plotted next in Figure 34 to get a clearer exhibition of their trapping behaviour.
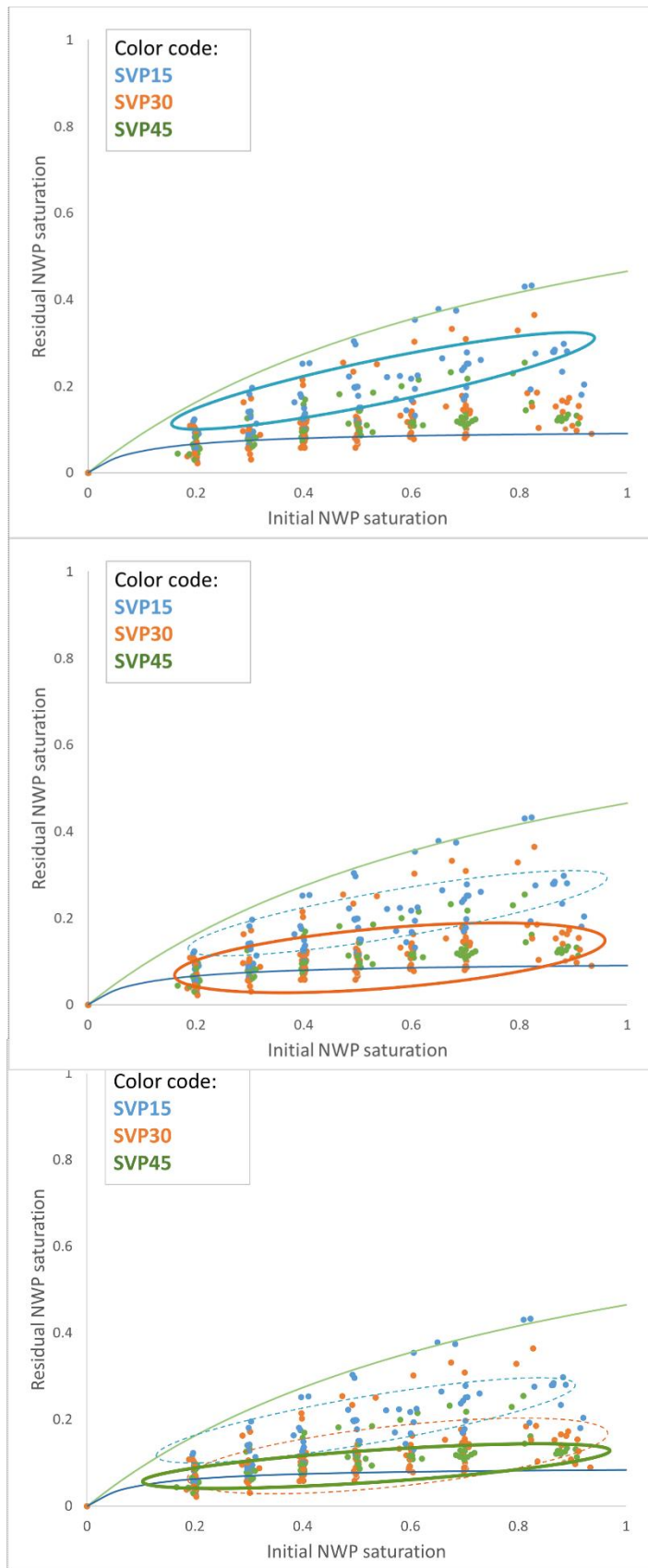
Figure 32. Grouping of trapping curves on SVP basis. Clear downtrend in capillary trapping with SVP increment.
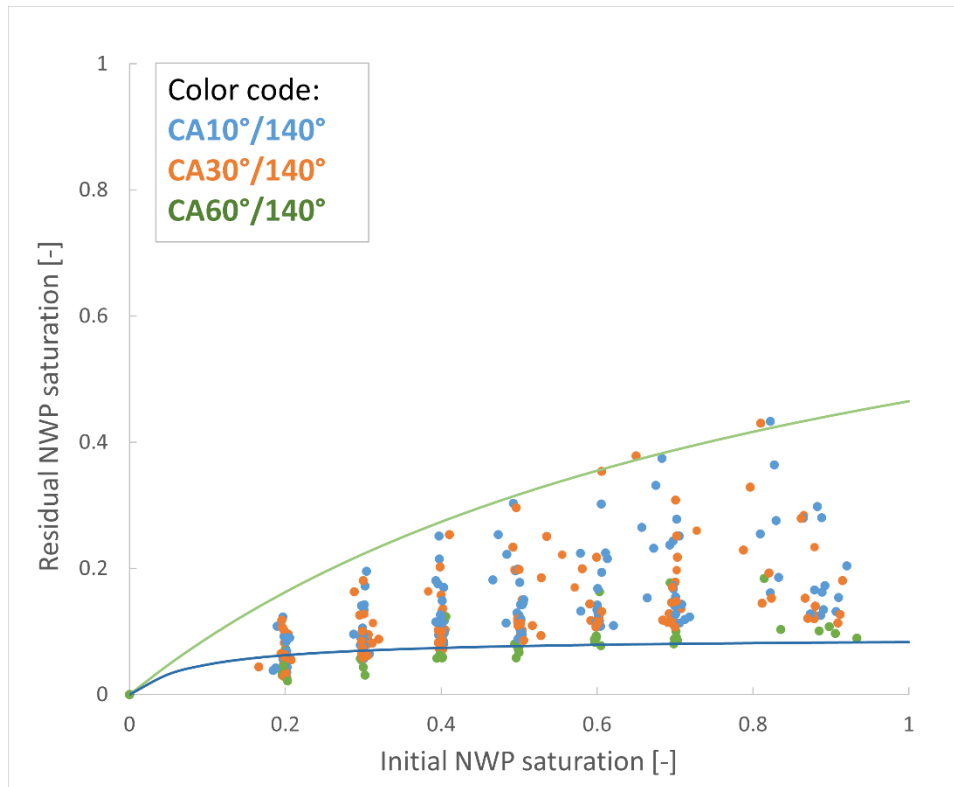
Figure 33. Grouping of trapping curves by CA.
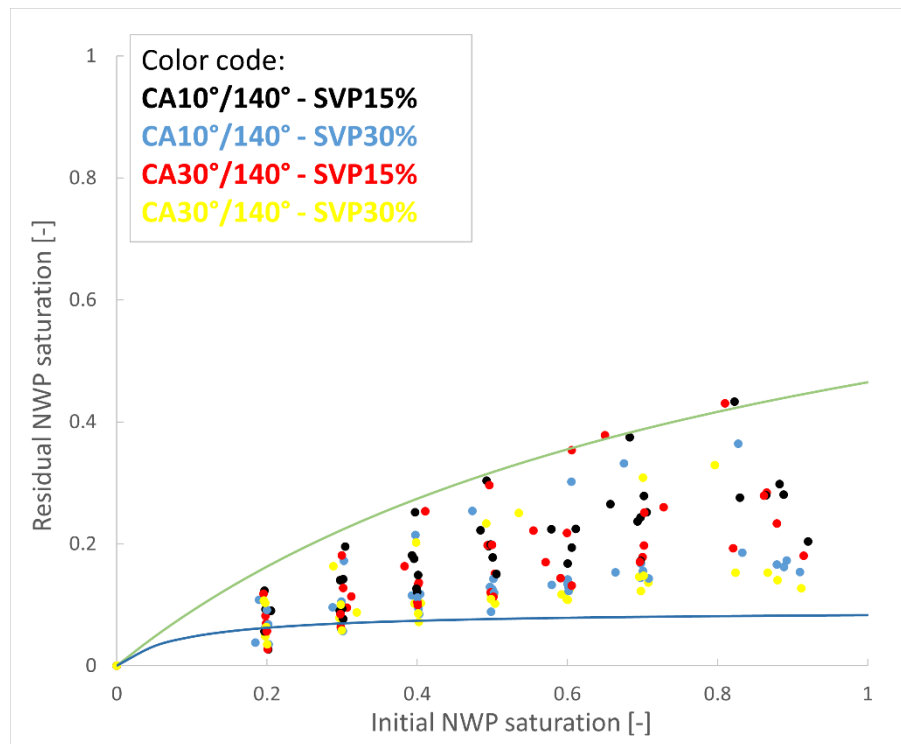
Figure 34. Plot of trapping curves from cases suggested to exhibit physical trapping behaviour.

Figure 34 shows distinctive trends in trapping curves. Except for outliers seen in the top part of the Land boundary, there is clear difference between black/red (SVP15) and yellow/blue (SVP30) trends, which clearly solidifies the influence of SVP over CA assigned. Even the outliers in the top part exhibit lesser degree of trapping when SVP30 is used. However, it has to be mentioned that SVP15 or lesser gives virtually non-existent forced imbibition part of imbibition branch. Important observation is that outliers in this results' configuration are from Sand_3.

When comparing Sand_3 trapping potential to other samples, the assumption is that clearest distinction comes in CA60°/140°-SVP30% case where the applied CA settings have shifted the wetting state so that only trapping comes from the effect pore structures have. Note that difference in trapping potential between Sand_3 and other samples is observed for other cases as well, however in other cases the trapping potential is influenced by applied settings more than in this one. Observations distinguished in Figure 35 show that trapping curve for Sand_3 is not following the same trend as other samples. As mentioned, it is presumed that crucial difference comes from Sand_3 pore geometry. Note that although trapping curves of other samples seem to be tightly aligned, there is still considerable variation of their Land constants from 7.5 to 10. In-depth analysis of pore structures is later presented to verify on this observation and the real impact pore geometries have. Figure 36 Figure 36shows trapping curves on sample-by-sample comparison to get a better understanding of trapping potential that structure geometry may have.
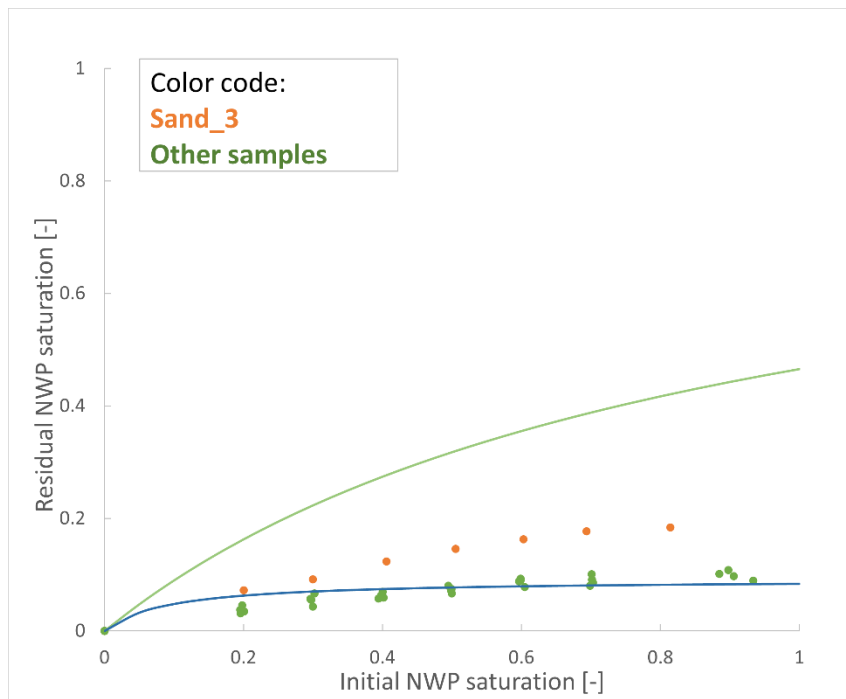
Figure 35. Case CA60°/140° SVP 30 shown for Sand_3 and other samples. Other samples follow the similar trend, while Sand_3 has clearly larger trapping.

Figure 36 shows that the comparison between samples makes the distinguishable difference. Qualitatively ranking, Sand_3 exhibits largest capillary trapping potential, while Sand_1 lowest. Other samples are somewhere in between without a clear difference. In any case, the effect of uncertainty added to sample by changing the CA and SVP seems to follow the general sample's trend in trapping. Sand_3 results exhibit larger trapping than rest of the samples in all but 1 case. This implies its pore properties have played the most significant role with application of PMM.

Finally, qualitative comparison of results with (Krevor et al. 2015) database is plotted in Figure 37. This comparison served as the initial motivation for development of this workflow and to investigate the applicability in CCS. As the results are not clearly comparable, reasons why have to be considered.
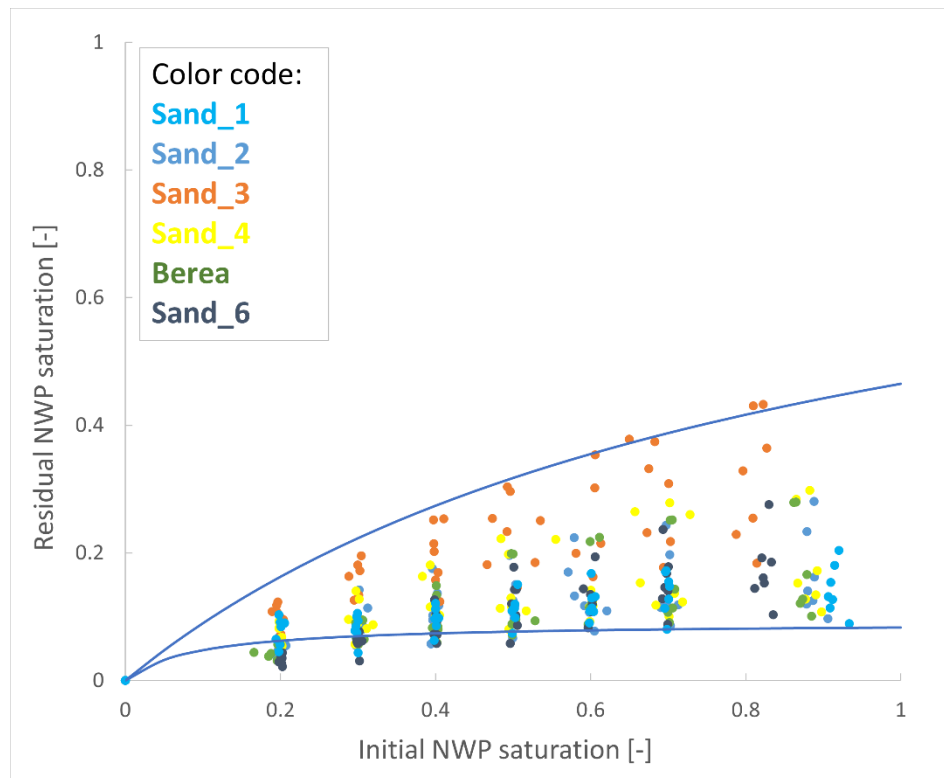
Figure 36. Trapping curves now presented on a sample-by-sample analysis. Certain trends are clear: Sand_3 is a sample with overall largest trapping potential obtained in this study. Sand_1, on the other hand, depicts overall smallest degree of capillary trapping.
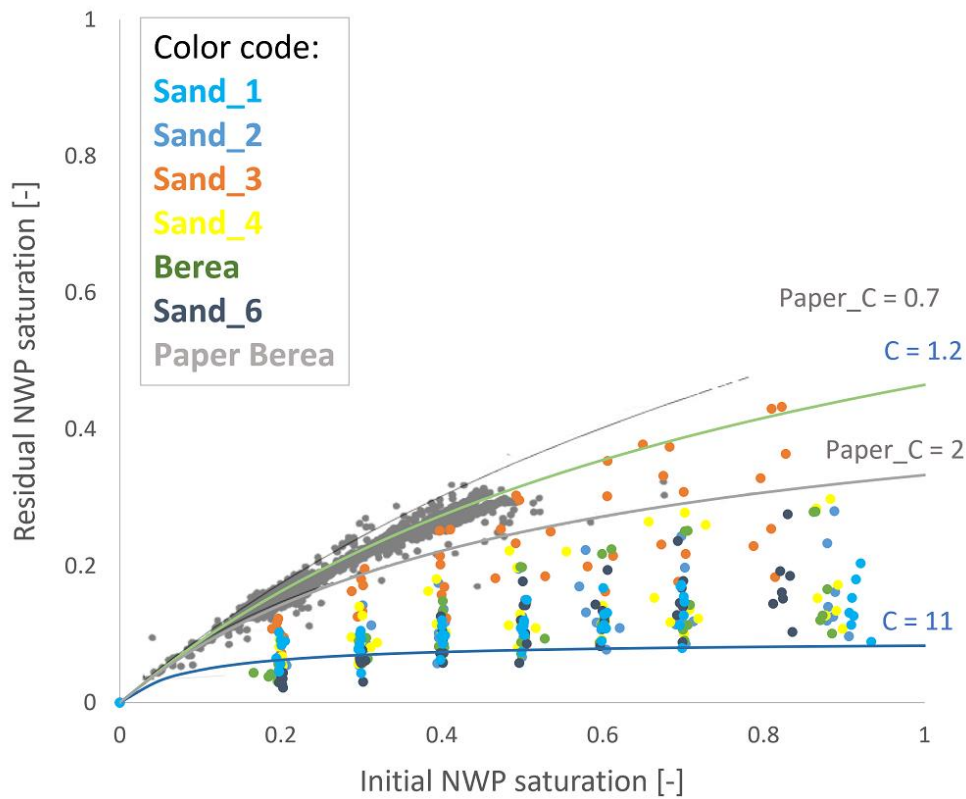
Figure 37. Data range in this study compared to data range for Berea sandstones in Krevor et al. 2015. Sand_3 results are the only in the paper range, and they are achieved in SVP15/30 and CA10/30 cases.

4.3 Domain and voxel size influence

A potential issue for the mismatches of the simulated and experimental Berea data might come from the limited domain size, which may also affect the early turning-saturations. Importance of Berea sample was already elaborated as a connection of this and other studies, and therefore additional investigation is conducted with a new Berea digital structure, named Berea_2 and seen in Figure 38. Its voxel size is 3.4 μm, which makes it comparable to other samples, while different to original Berea thus allowing the investigation of domain and voxel size, as well as the pore structure properties. Additional investigations with a new sample focus on the case most comparable to literature experimental data, which is CA30°/140°_SVP15%. The trapping curve for Berea_2 is presented in Figure 39 and is compared to original Berea results and literature Land-parameter range observed in experiments for Berea.

Figure 38. Berea_2 structure, used for deeper insight and relation of this and other studies using Berea.
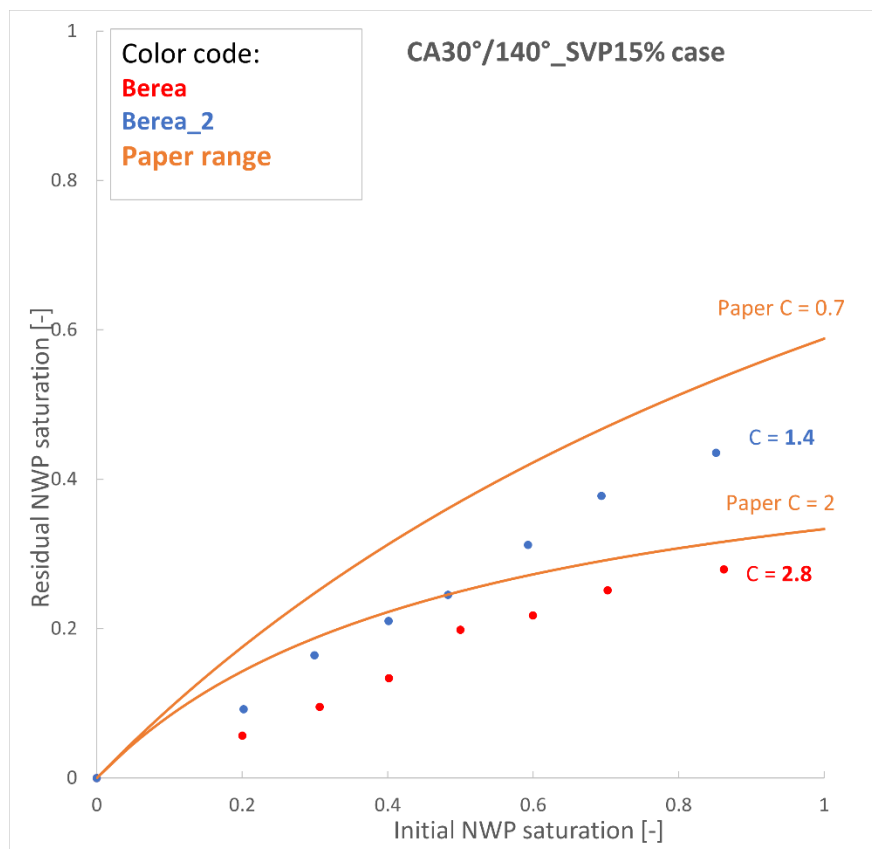
Figure 39. Comparison of trapping results for Berea and Berea_2 structures with literature range. Land model was fitted to simulated results (dots) and C values are expressed in figure.

Land-models is fitted to simulated results for Berea and Berea_2 and Land-parameter values are C = 1.4 and C = 2.8, respectively. Results show that a new Berea_2 structure exhibits

considerably larger capillary trapping compared to original Berea and also the majority of other sandstone structures used in the thesis. Land model is fitted to match the results for Berea_2 with Land-parameter C = 1.4. This value, as can be seen in above figure, now lies inside the observed range from literature. However, the observed behaviour is still not correctly matched by application of Land model. The largest discrepancy between the Land model and observed simulated results is seen for early turning-saturation IR pairs, and implication is that morphological approach applied on rock structures doesn't correctly resolve this region. There are different implications for such behaviour that will be discussed and tackled. One of the issues may lie in structure domain size.

In this study, simulations were limited to domain size of 500^3 voxels. Main limiting factor for using the larger domains in simulations is considerably longer runtime, arising from cubic increase of domain size/voxels. That is why it was out of scope to conduct such simulations for all rock structures and cases initially. The 500^3-voxel domain corresponds to rock structures being in millimetre-scale. For such small simulation domains, there is the possible issue of numerical boundary and capillary-end effects. These effects are deemed to subsequently result in nonphysical saturations and consequent mismatch of Land model with simulated data. The reason for such boundary effects revolves around the connectedness of NW phase to NWP reservoir during imbibition process, and inefficiency of morphological approach to adequately resolve saturation distribution in the near NWP-reservoir region. This effect is extrapolated if domain size is small, and is especially seen at early-saturation scanning imbibition turning points. Additionally, in literature experimental data the corefloods are conducted on much larger sample sizes. There is the difference from this study – millimetre-scale – with the experimental results – centimetre-scale – that may also be one of potential issues when comparing Land trapping curves.

To investigate the correlation with domain size, additional simulations were performed on a larger domain of 1000^3 voxels. Increasing the domain size shall tackle both the boundary condition effects as well as include more realistic pore size distribution. Both Berea structures are used for investigations as they are same rock type that is supposed to exhibit similar trapping potential. However, that may not be the case due to different reasons. For instance, Berea properties are still varying in a substantial range that may yield considerable differences. This heterogeneity in properties is further distinguished at millimetre range, and these samples are at that scale. Also, differing scanning and acquisition methods used in creation of digital rocks may have induced additional discrepancies. The parameter combination used in simulations is chosen as follows, CA30°/140°_SVP15%, since this combination exhibited the most realistic results so far. This case in particular shows the most realistic trapping compared to literature data. Additionally, for Berea 1000^3-domain cases of CA10°/140°_SVP15% and

CA60°/140°_SVP15% are investigated for additional insight into the effect of CA on large domain.

The results on Berea structure for different cases on the large domain with the Land fits are plotted in Figure 40. There is virtually no difference between CA10°/140° and CA30°/140° cases, but significant difference with CA60°/140° case. This is in agreement with previous observations on a small domain. Further results will focus on CA30°/140° case. A major observation is the impact the domain size has on the capillary trapping, as the fitted Land parameter is now 1.5, which is considerably more in line with the literature data.
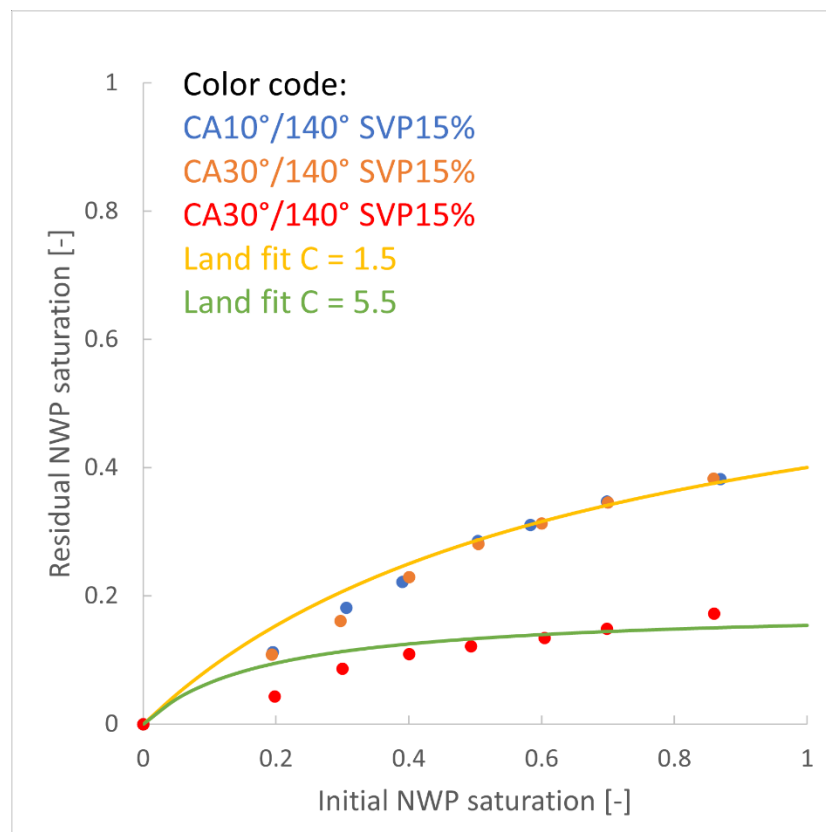
Figure 40. Berea original sample: 1000³-voxel domain simulations of different cases with Land fits. Cases for CA10°/140° and CA30°/140° show almost identical behaviour.

However, early data points are still below the Land-model line fit, which may indicate that the modelling approach is insufficient to properly capture early saturation ranges. This can be due to already mentioned issues, such as inadequacy of morphological approach to effectively resolve the boundary-end effects. Therefore, the use of mirrored domain is used as a next approach to tackle this issue.

For mirrored-domain approach, orientations of NWP/WP reservoirs are most important, therefore the domain was mirrored in Z-direction to observe the impact boundary effects may have. The imbitition and drainage are simulated on the fully extended domain, whereas the

saturations are checked on both the full domain and the initial structure as well. As simulation turns to imbibition, invading phase is from Z- side. The most of the boundary-end artefacts are expected near the NWP reservoir, which is then at Z+ side. It is proposed that all the results for this mirrored approach are observed at Z- side, as this side is not relying on connectedness to NWP during imbibition, thus not supposed to exhibit boundary end effects, as elaborated in workflow. The results on Berea structure comparing original domain size, fully extended (mirrored) domain, and different cutoff parts of complete domain are shown in Figure 41.
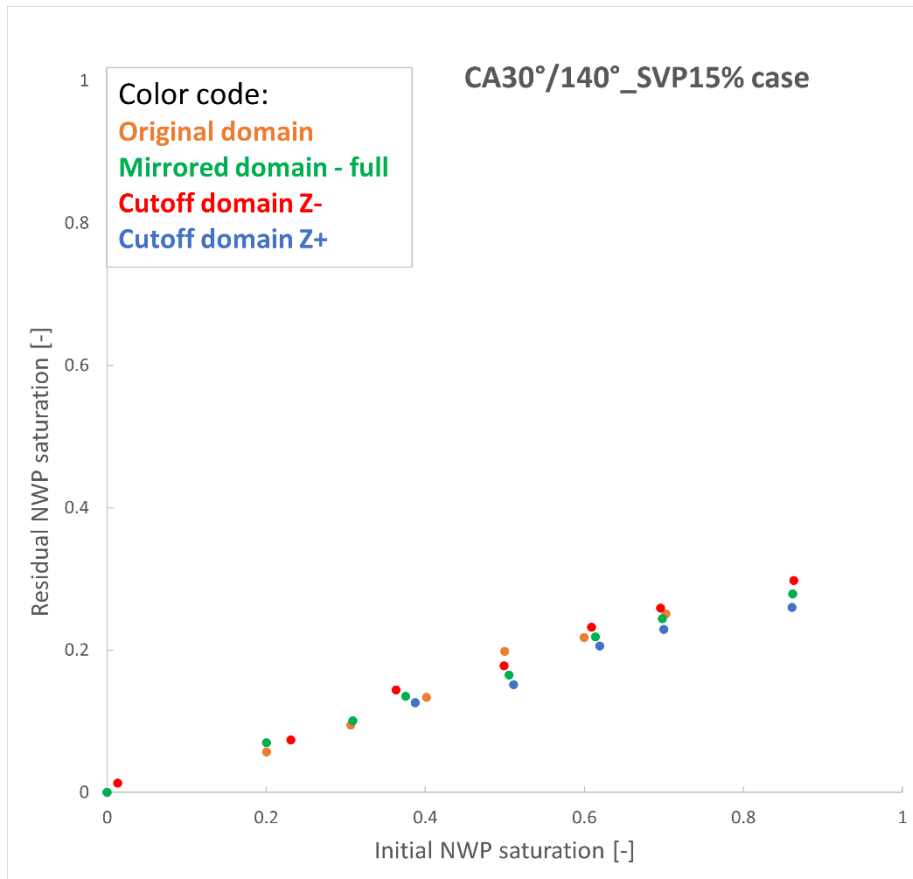
Figure 41. Comparison of trapping curves created from different parts of mirrored domain, including complete mirrored domain and original, unmirrored domain curve.

There is inconsistent behaviour seen for each of the used approaches with mirrored domain. If the results are observed for a fully extended/mirrored domain, there is the improvement of trapping behaviour trend at some of the early turning saturations – 0.2, 0.3, and 0.4 compared to original domain. Improvement is minor, whereas at later turning saturations the trend is unclear and there seems to be a shift in trapping, and original domain showing larger trapping than extended/mirrored. Also, there are observed issues with cutoff approach at early turning saturations. Namely, the drainage invasion side – Z+ - gets mainly invaded by NWP, while there is almost no invasion yet in the extended part of Z domain – Z-. This process is observed at NWP turning saturations of 0.2, 0.3, and 0.4. At higher turning saturations, the invasion of Z-

domain is consistently increasing until the irreducible WP saturation, when it is virtually equal to complete domain. Extended domain approach for Z- side cutoff is compared with large domain, original domain and the literature data range in Figure 42.
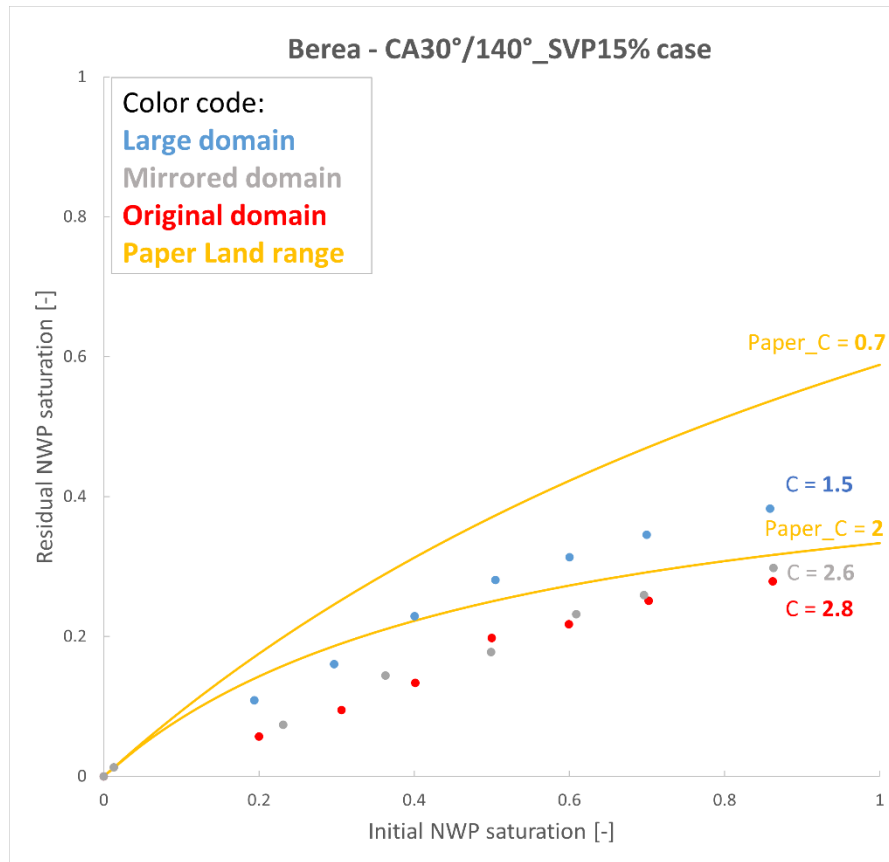
Figure 42. Comparison of domain size influence on trapping curves for Berea. There is the considerable influence of domain size (large domain case), and there is unclear influence of boundary-end effects (mirrored domain).

Although showing influence, mirrored domain approach yields rather unclear effect. Overall trapping is slightly improved with a shift of Land parameter from 2.8 to 2.6. Early stage behaviour also shows slightly better performance. However, there is still a considerable gap between early turning saturations and the Land-model fit. It may be considered that near-NWP reservoir region, thought to have a large impact on boundary numerical errors, is not the main cause of early-points mismatch. Finally, comparison of Berea and Berea_2 samples with original-size domain and large 1000^3 domain is shown in Figure 43 for additional insight of domain size impact. Land model is fitted to both curves and for Berea the shift in C value from small to large domain is from 2.8 to 1.5, while for Berea_2 C values shifts from 1.4 to 0.8. Interestingly, for both Berea structures the large domain trapping potential is now in literature range from (Krevor et al. 2015). This may indicate the improvement larger simulation domains bring in description of capillary trapping. However, early turning-saturations are for both cases

out of the Land model, which has to be addressed in future studies. Also, additional investigation of large domain simulations with other samples should be conducted to gain further insight of domain-size impact.
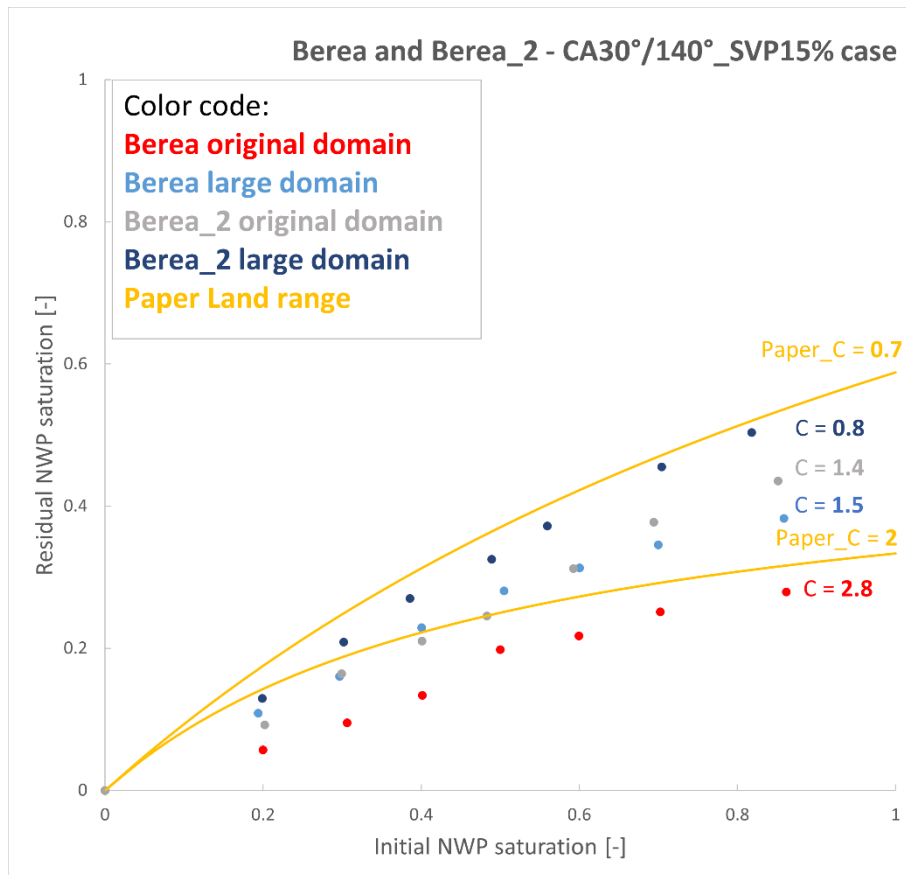
Figure 43. Comparison of trapping potential for large vs. small domains with Berea and Berea_2 structures. For additional insight, literature range for Berea is plotted to indicate the improvement large domain simulations bring in description of trapping potential.

4.4 Correlation of petrophysical properties and trapping potential

Figure 36 and Figure 39 have indicated that the rock type has a significant influence on the trapping potential, therefore the effect of the intrinsic rock properties on the Land parameters is explored. The following investigations include different aspects of pore analysis with PoroDict module in Geodict.

Petrophysical analysis is conducted with the simulation results from 500^3 domain for all samples. First, trapping curves for a base case across different samples are presented in Figure

44. Base case is same as used in investigation of domain size, CA30°/140° SVP15%. This case in particular has more realistic trapping properties than other simulated cases, thus is here used for analysis.
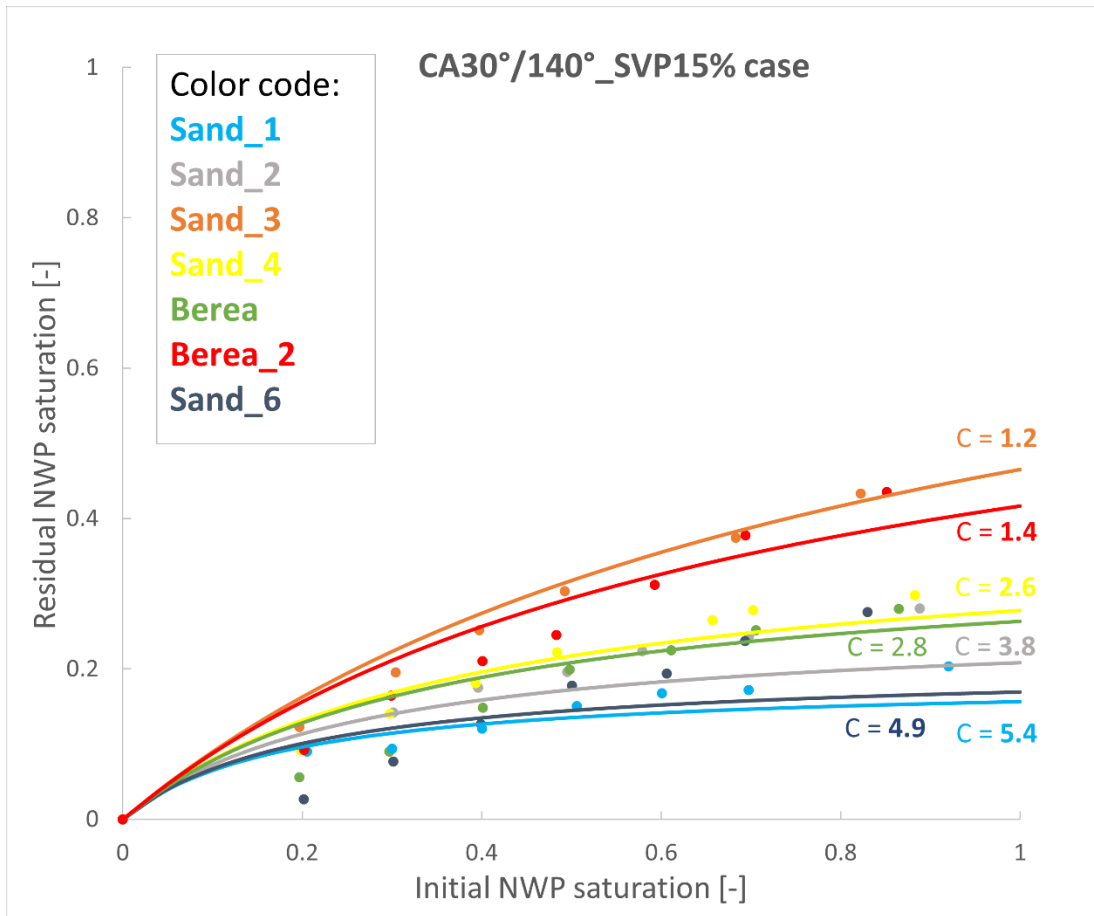
Figure 44. Land curves fitted to data points for case CA30°/140°_SVP15. Fit with sum of least squares method.

Best-fit Land-model parameters along with respective petrophysical properties are given in Table 3. Plotted relationships between Land parameters and respective petrophysical properties is following to make a clearer, visual distinction. Plots are compared to each other and include all the properties in table, which are porosity, permeability, coordination number, pore throat distribution, and pore body size distribution.

Table 3. Land parameters and petrophysical properties of respective rock structures used in this study.

	Sand_1	Sand_2	Sand_3	Sand_4	Sand_6	Berea	Berea_2
Land-parameters	**5.4**	**3.8**	**1.2**	**2.6**	**4.9**	**2.8**	**1.4**
Porosity	0.263	0.283	0.187	0.318	0.159	0.182	0.182
Permeability	15600	2870	624	2468	1210	498	1381
Coordination number, mean	2.906	4.05	3.33	4.633	1.755	3.03	2.697
Pore throat size distribution - characteristic diameter, µm							
D10	23.7	12.8	9.04	10	15.4	5.5	15.2
D50	64.2	29.3	18.03	18.8	47.9	17.5	30.8
D90	99.4	44.6	23.97	28.1	99.4	44.7	51.9
Pore size distribution - characteristic diameter, µm							
D10	24.9	14.4	10.4	10.66	17.61	6.15	16.75
D50	78.9	34.6	23.1	23.97	56.7	21.6	41.7
D90	145.6	67.6	43.4	42.5	128.7	57.1	80.2
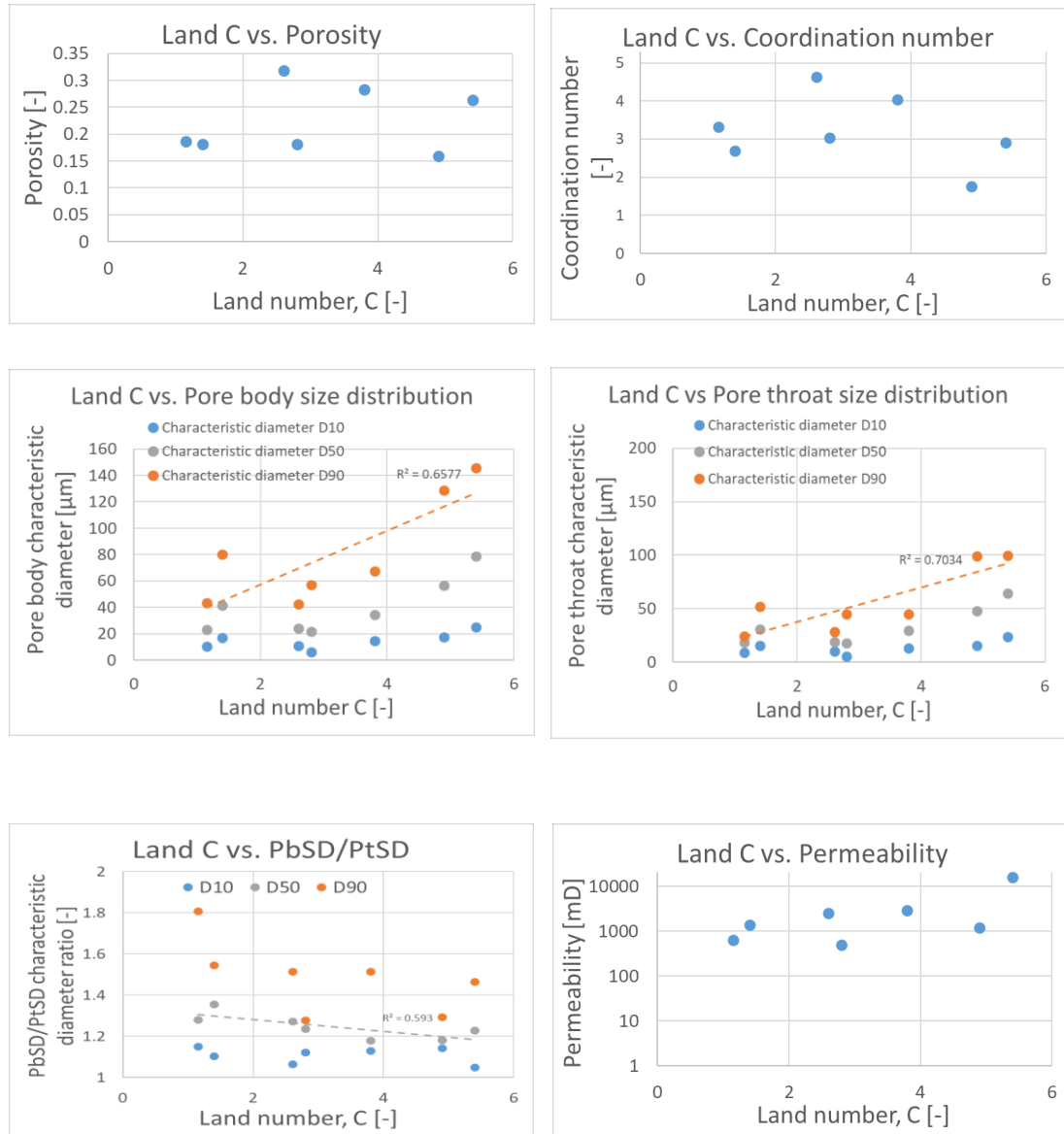
Figure 45. Cross-comparison of different petrophysical properties plotted against Land parameters for respective structures used in this study.

Top row in above figure shows porosities and coordination numbers plotted against respective Land-model parameters. There is no clear trend. For porosity plot, Sand_3 and Berea_2 have best overall trapping behaviour, whereas Sand_4 and Sand_6 have similar or lower porosities and considerably worse observed trapping. When trying to fit a linear trendline, R-squared coefficient of determination is 0.041. However, it has to be noted that literature shows similar discrepancies in results when comparing samples of wide variation in properties, which here may be the case as well (Andersson et al. 2018). Plot for coordination number shows substantially similar pattern in data behaviour to C-porosity plot. Both of them display no exact linear relation between Land parameters and investigated petrophysical property. Sand_6, for

instance, has the lowest coordination number, while it has much worse trapping potential than the other samples. Similar trend is for Sand_1. One observation is that other samples without Sand_1 and Sand_6 show a potential linear trend that is considered physical – there is lesser degree of trapping with larger coordination number. With a linear trendline, R-squared is 0.09.

Next two plots show pore body and pore throat size distributions against Land parameters. Distribution are expressed with D10, D50, and D90 characteristic diameters that are larger than 10%, 50%, and 90% of all pore diameters, respectively. Both distributions show high-degree of mutual correlation, and comparing them to trapping shows increasing relationship as distribution range increases from D10 to D90. D90 characteristic diameter particularly shows the relationship with trapping potential, for both throat and body distributions. With linear trendlines, R-squared coefficients of determination are 0.70 and 0.66 for pore throat and body size distributions, respectively. The ratio of pore body and pore throat distribution gives the estimate of pore aspect ratio at certain statistical ranges. There is a correlation of 0.59 with Land parameters. However, as previously mentioned, aspect ratio derived with statistical approach cannot be taken as a proper estimate of true pore aspect ratio, and this has to be acknowledged. Rather, direct calculation of aspect ratio with simulation tool should be implemented for clearer connection with trapping potential.

In plot for C – permeability relationship, the Y-axis (permeability) has to be adjusted with logarithmic scale to accommodate for large difference of Sand_1, which has permeability by the factor of 10 larger than other samples. However, Sand_1 showed the behaviour in same direction as the other structures, namely that the higher structures' permeability is linked with larger Land parameter – lower capillary trapping potential. Berea and Sand_6, however, show considerably different trend compared to other samples. One similarity between these two samples is that their pore size distributions have the highest degree of heterogeneity compared to other samples.

Final remarks are that although unclear, there are observed trends in trapping potential and petrophysical properties, which may require deeper investigation in future studies to exactly resolve the correlations. There seems to be the pattern and mutual relationship between petrophysical properties and Land constants, and most likely they should be considered as a whole, where each of the properties combined with others describes the correct trend in capillary trapping.

Chapter 5

Conclusion

5.1 Summary

As part of global carbon emissions reduction, field of CCS provides the opportunity of safely storing carbon dioxide in deep reservoirs and saline aquifers. Capillary trapping is a major component of overall trapping mechanisms, and as such requires deep analysis for assurance of long-term safety of storage. Special Core Analysis is used to describe rock properties needed for capillary trapping, but it requires significant effort due to its complexity and time, as well as numerous unknowns impacted by rock heterogeneity. With the advance of digital computing and implementation of realistic processes in simulation toolboxes, field of Digital Rock Physics (DRP) promises substantial improvement in description of trapping processes.

The capillary trapping potential of different rock types was investigated in this study with the applied DRP software Geodict. It is of major interest for future applicability in potential CCS projects. Literature was used as a reference for understanding of simulated and experimental results in the fields of CCS and pore morphology simulations. Six different digital rock samples were used in investigation, providing variation in the pore structures. In Geodict, Satudict module was of particular importance, which applies pore morphology method for simulation of capillary processes. Trapping curves with Land model were fitted to the simulated capillary pressure curves to describe trapping potential of each rock structure, and to make the results in this study comparable with other studies using Land model. Simulation of capillary processes required proper modelling of drainage and imbibition to realistically describe the hysteretic capillary pressure-saturation cycles that impact the trapping.

The workflows applied in this thesis investigated two approaches for imbibition modelling in Geodict. The standard approach modelled only the spontaneous imbibition and allowed for variation of contact angle applied, which was done to model the uncertainty related to wetting conditions. The resulting trapping curves showed unclear trends, without a proper correlation between applied contact angles and observed trapping. This was presumed to be the case due to missing part of forced imbibition, as earlier zero-crossing (shift from spontaneous to forced imbibition) occurs with larger contact angles. Trends in trapping were observed on a sample-

by-sample comparison, thus implying the impact pore structure has. However, the relationship between samples properties and trapping didn't follow the expected relationship. Also, qualitative comparison with literature data showed higher capillary trapping potential with the standard approach than observed in literature experimental results.

The improved approach included a new implementation that simulates spontaneous and forced imbibition – full imbibition branch. To apply this approach, rock structures required modification to consist of two materials of water and non-wet contact angles due to the forced imbibition being modelled as inverse drainage. Second NW material was implemented with a statistical distribution to allow for a homogeneous effect on capillary processes. Trapping curves developed with new approach were analysed according to contact angles applied and the amount of secondary material implemented. Amount of secondary material applied showed a major influence, therefore its applicability is revised for future studies. Literature data range of Land-model parameters served as a qualitative benchmark. It showed the considerable mismatch also with a new approach, but now lesser capillary trapping potential. Additional investigations on a previously-used and additional Berea digital structures observed the impact that a simulation domain size has, with Land-model parameter now matching the literature range. It may be concluded that the most significant impact on trapping potential is due to the amount of SVP applied, and the simulation domain size. Former has a major impact on wetting state, while latter changes the representative elementary volume that the simulation is run at. Also, extended simulation domain was used to explicitly target boundary end-effects that were thought to impact early IR turning saturation pairs. However, neither large nor extended domain completely resolved this issue, with only a minor improvement observed within extended-domain results. The samples' petrophysical properties were examined and correlated with fitted Land-model parameters. Although not fully clear, trends in capillary trapping were seen with the pore body and pore throat size distribution. The trends were most clearly visible when the correlation involved trapping and characteristic pore diameter that is larger than 50% of all pore diameters.

As a conclusive remark, this workflow managed to tackle the creation of trapping curves in Geodict. Certain assumptions have to be acknowledged when applying it, as certain physical processes are still not captured within the morphological approach and show trends not expected to be seen in water-wet conditions. Better understanding of capillary trapping processes was obtained with additional petrophysical analysis, and the better match in trapping results was observed with increased simulation domain. Further studies combining this workflow and experimental results with same samples should yield additional improvements, and additional implementations in fields of morphological simulations will lead towards realistic observations.

5.2 Future Work

Different digital rock samples were used in this study, which gave an insight into the connection between rock geometry and observed capillary pressure and trapping behaviour. However, it was also observed how the issue of domain size plays a role. There was a considerable difference in the observed behaviour for the same sample in two different domain sizes. Further studies should tackle this issue and address all the used digital rock structures on the larger domain. Also, recommendation is to apply lesser amounts of secondary NW material, to match the rock wettability more precisely.

Observations of simulated trapping curves showed considerable degree of mismatch between early initial-residual turning-saturation pairs and fitted Land model. As different approaches to tackle this with domain modification haven't yielded the better fit, further investigation should focus here. Probable solutions should tackle direct implications of morphological approach and incorporate more realistic experimental observations. Also, the interaction of CO_2 with brine is here of interest, as there are special considerations for CO_2 dissolution in brine and CO_2-trapping mechanisms that are not precisely addressed with current Geodict capabilities.

Additionally, implementation for pore body-to-throat aspect ratio in Geodict should be derived. This parameter is considered to have a substantial impact on capillary trapping, therefore correlation of aspect ratio with trapping could lead to additional insight.

Finally, further step should be revision of used empirical models and their impact on relative permeabilities. Namely, there are different relative permeability models applied to either water-wet or mixed/oil-wet reservoirs, and for exact purposes of relative permeability description, appropriate models should be applied.

Chapter 6

References

Akbarabadi, Morteza; Piri, Mohammad (2013): Relative permeability hysteresis and capillary trapping characteristics of supercritical CO2/brine systems: An experimental study at reservoir conditions. In *Advances in Water Resources* 52, pp. 190–206. DOI: 10.1016/j.advwatres.2012.06.014.

Alexandru-Mihai Badescu (2020): Digital Rock Physics for Unconsolidated Sandstones – A Grain Size Distribution Approach. Master thesis.

Al-Menhali, Ali; Krevor, Samuel (2014): Effective Wettability Measurements of CO2-brine-Sandstone System at Different Reservoir Conditions. In *Energy Procedia* 63, pp. 5420–5426. DOI: 10.1016/j.egypro.2014.11.572.

Al-Menhali, Ali S.; Krevor, Samuel (2016): Capillary Trapping of CO2 in Oil Reservoirs: Observations in a Mixed-Wet Carbonate Rock. In *Environmental science & technology* 50 (5), pp. 2727–2734. DOI: 10.1021/acs.est.5b05925.

Andersson, Linnéa; Herring, Anna; Schlüter, Steffen; Wildenschild, Dorthe (2018): Defining a novel pore-body to pore-throat "Morphological Aspect Ratio" that scales with residual non-wetting phase capillary trapping in porous media. In *Advances in Water Resources* 122, pp. 251–262. DOI: 10.1016/j.advwatres.2018.10.009.

Bakke, Stig; Øren, Pål-Eric (1997): 3-D Pore-Scale Modelling of Sandstones and Flow Simulations in the Pore Networks. In *SPE Journal* 2 (02), pp. 136–149. DOI: 10.2118/35479-PA.

Bennion, Brant; Bachu, Stefan (2008): Drainage and Imbibition Relative Permeability Relationships for Supercritical CO2/Brine and H2S/Brine Systems in Intergranular Sandstone, Carbonate, Shale, and Anhydrite Rocks. In *SPE Reservoir Evaluation & Engineering* 11 (03), pp. 487–496. DOI: 10.2118/99326-PA.

Benson, Sally M.; Orr, Franklin M. (2008): Carbon Dioxide Capture and Storage. In *MRS Bull.* 33 (4), pp. 303–305. DOI: 10.1557/mrs2008.63.

Berg, S.; Rücker, M.; Ott, H.; Georgiadis, A.; van der Linde, H.; Enzmann, F. et al. (2016): Connected pathway relative permeability from pore-scale imaging of imbibition. In *Advances in Water Resources* 90, pp. 24–35. DOI: 10.1016/j.advwatres.2016.01.010.

Blunt, M. J. (2000): An Empirical Model for Three-Phase Relative Permeability. In *SPE Journal* 5 (04), pp. 435–445. DOI: 10.2118/67950-PA.

Blunt, Martin J.; Bijeljic, Branko; Dong, Hu; Gharbi, Oussama; Iglauer, Stefan; Mostaghimi, Peyman et al. (2013): Pore-scale imaging and modelling. In *Advances in Water Resources* 51, pp. 197–216. DOI: 10.1016/j.advwatres.2012.03.003.

Bryant, Steven L.; King, Peter R.; Mellor, David W. (1993): Network model evaluation of permeability and spatial correlation in a real random sphere packing. In *Transp Porous Med* 11 (1), pp. 53–70. DOI: 10.1007/BF00614635.

El-Maghraby, Rehab M.; Blunt, Martin J. (2013): Residual CO2 trapping in Indiana limestone. In *Environ. Sci. Technol.* 47 (1), pp. 227–233. DOI: 10.1021/es304166u.

Farokhpoor, Raheleh; Bjørkvik, Bård J.A.; Lindeberg, Erik; Torsæter, Ole (2013): Wettability behaviour of CO2 at storage conditions. In *International Journal of Greenhouse Gas Control* 12, pp. 18–25. DOI: 10.1016/j.ijggc.2012.11.003.

Hazlett, R. D. (1995): Simulation of capillary-dominated displacements in microtomographic images of reservoir rocks. In *Transp Porous Med* 20 (1-2), pp. 21–35. DOI: 10.1007/BF00616924.

Hilpert, Markus; Miller, Cass T. (2001): Pore-morphology-based simulation of drainage in totally wetting porous media. In *Advances in Water Resources* 24 (3-4), pp. 243–255. DOI: 10.1016/S0309-1708(00)00056-7.

Holm, L. W.; O' Brien, L. J. (1971): Carbon Dioxide Test at the Mead-Strawn Field. In *Journal of Petroleum Technology* 23 (04), pp. 431–442. DOI: 10.2118/3103-PA.

Hu, Ran; Wan, Jiamin; Kim, Yongman; Tokunaga, Tetsu K. (2017): Wettability impact on supercritical CO 2 capillary trapping: Pore-scale visualization and quantification. In *Water Resour. Res.* 53 (8), pp. 6377–6394. DOI: 10.1002/2017WR020721.

IEA (2021.): Energy Policies of IEA Countries: Norway 2005 – Analysis - IEA. Available online at https://www.iea.org/reports/energy-policies-of-iea-countries-norway-2005, updated on 8/8/2021., checked on 8/8/2021.

IOGP Publications library (2021.): Map of global CCUS projects | IOGP Publications library. Available online at https://www.iogp.org/bookstore/product/map-of-global-ccs-projects/, updated on 8/8/2021., checked on 8/8/2021.

Killough, J. E. (1976): Reservoir Simulation With History-Dependent Saturation Functions. In *Society of Petroleum Engineers Journal* 16 (01), pp. 37–48. DOI: 10.2118/5106-PA.

Krevor, Samuel; Blunt, Martin J.; Benson, Sally M.; Pentland, Christopher H.; Reynolds, Catriona; Al-Menhali, Ali; Niu, Ben (2015): Capillary trapping for geologic carbon dioxide storage – From pore scale physics to field scale implications. In *International Journal of Greenhouse Gas Control* 40, pp. 221–237. DOI: 10.1016/j.ijggc.2015.04.006.

Krevor, Samuel C. M.; Pini, Ronny; Zuo, Lin; Benson, Sally M. (2012): Relative permeability and trapping of CO_2 and water in sandstone rocks at reservoir conditions. In *Water Resour. Res.* 48 (2). DOI: 10.1029/2011WR010859.

Land, Carlon S. (1968): Calculation of Imbibition Relative Permeability for Two- and Three-Phase Flow From Rock Properties. In *Society of Petroleum Engineers Journal* 8 (02), pp. 149–156. DOI: 10.2118/1942-PA.

Larsen, J. A.; Skauge, Arne (1998): Methodology for Numerical Simulation With Cycle-Dependent Relative Permeabilities. In *SPE Journal* 3 (02), pp. 163–173. DOI: 10.2118/38456-PA.

Lenhard, R. J.; Oostrom, M. (1998): A Parametric Model for Predicting Relative Permeability-Saturation-Capillary Pressure Relationships of Oil–Water Systems in Porous Media with Mixed Wettability. In *Transport in Porous Media* 31 (1), pp. 109–131. DOI: 10.1023/A:1006503406056.

Lenormand, R.; Zarcone, C.; Sarr, A. (1983): Mechanisms of the displacement of one fluid by another in a network of capillary ducts. In *J. Fluid Mech.* 135 (-1), p. 337. DOI: 10.1017/S0022112083003110.

Li, Xuesong; Boek, Edo; Maitland, Geoffrey C.; Trusler, J. P. Martin (2012): Interfacial Tension of (Brines + CO_2): (0.864 NaCl + 0.136 KCl) at Temperatures between (298 and 448) K, Pressures between (2 and 50) MPa, and Total Molalities of (1 to 5) $mol \cdot kg$ –1. In *J. Chem. Eng. Data* 57 (4), pp. 1078–1088. DOI: 10.1021/je201062r.

Mario Stefan Dragovits (2021): Uncertainty ranges of Uncertainty ranges of simulated capillary pressure curves. Master thesis. Montanuniversität Leoben.

Math2Market GmbH; Hilden, Janine; Rief, Sebastian; Planas, Barbara (2020): GeoDict User Guide - GrainGeo 2021: Math2Market GmbH.

Niu, Ben; Al-Menhali, Ali; Krevor, Samuel C. (2015): The impact of reservoir conditions on the residual trapping of carbon dioxide in Berea sandstone. In *Water Resources Research* 51 (4), pp. 2009–2029. DOI: 10.1002/2014WR016441.

Pentland, Christopher H.; El-Maghraby, Rehab; Iglauer, Stefan; Blunt, Martin J. (2011): Measurements of the capillary trapping of super-critical carbon dioxide in Berea sandstone. In *Geophys. Res. Lett.* 38 (6), n/a-n/a. DOI: 10.1029/2011GL046683.

Pentland, Christopher H.; Itsekiri, Endurance; Al Mansoori, Saleh K.; Iglauer, Stefan; Bijeljic, Branko; Blunt, Martin J. (2010): Measurement of Nonwetting-Phase Trapping in Sandpacks. In *SPE Journal* 15 (02), pp. 274–281. DOI: 10.2118/115697-PA.

Pit Arnold (2018): Experimental investigation of interfacial tension for alkaline flooding. Master thesis.

Planas, B. (2021.): About GeoDict. Available online at https://www.math2market.com/Solutions/aboutGD.php?=&Language=en, updated on 9/14/2021., checked on 9/14/2021.

Ruprecht, Catherine; Pini, Ronny; Falta, Ronald; Benson, Sally; Murdoch, Lawrence (2014): Hysteretic trapping and relative permeability of CO2 in sandstone at reservoir conditions. In *International Journal of Greenhouse Gas Control* 27, pp. 15–27. DOI: 10.1016/j.ijggc.2014.05.003.

Saraji, Soheil; Goual, Lamia; Piri, Mohammad; Plancher, Henry (2013): Wettability of supercritical carbon dioxide/water/quartz systems: simultaneous measurement of contact angle and interfacial tension at reservoir conditions. In *Langmuir : the ACS journal of surfaces and colloids* 29 (23), pp. 6856–6866. DOI: 10.1021/la3050863.

Schulz, Volker P.; Wargo, Eric A.; Kumbur, Emin C. (2015): Pore-Morphology-Based Simulation of Drainage in Porous Media Featuring a Locally Variable Contact Angle. In *Transp Porous Med* 107 (1), pp. 13–25. DOI: 10.1007/s11242-014-0422-4.

Spiteri, Elizabeth J.; Juanes, Ruben; Blunt, Martin J.; Orr, Franklin M. (2008): A New Model of Trapping and Relative Permeability Hysteresis for All Wettability Characteristics. In *SPE Journal* 13 (03), pp. 277–288. DOI: 10.2118/96448-PA.

Valvatne, Per H.; Blunt, Martin J. (2004): Predictive pore-scale modeling of two-phase flow in mixed wet media. In *Water Resour. Res.* 40 (7). DOI: 10.1029/2003WR002627.

W. Gunter; E. Perkins; T. McCann (1993): Aquifer disposal of CO2-rich gases: Reaction design for added capacity. In *undefined*. Available online at

https://www.semanticscholar.org/paper/Aquifer-disposal-of-CO2-rich-gases%3A-Reaction-design-Gunter-Perkins/b240f421ba36c5836b80b6de5c2fa0738bab98e4.

Whorton, Leonidas P.; Brownscombe, Eugene R.; Dyes, Alvin B. (2021.): US2623596A - Method for producing oil by means of carbon dioxide - Google Patents. Available online at https://patents.google.com/patent/US2623596A, updated on 7/27/2021., checked on 7/27/2021.

Xing, Wanli; Song, Yongchen; Zhang, Yi; Nishio, Masahiro; Zhan, Yangchun; Jian, Weiwei; Shen, Yong (2013): Research Progress of the Interfacial Tension in Supercritical CO2-water/oil System. In *Energy Procedia* 37, pp. 6928–6935. DOI: 10.1016/j.egypro.2013.06.625.